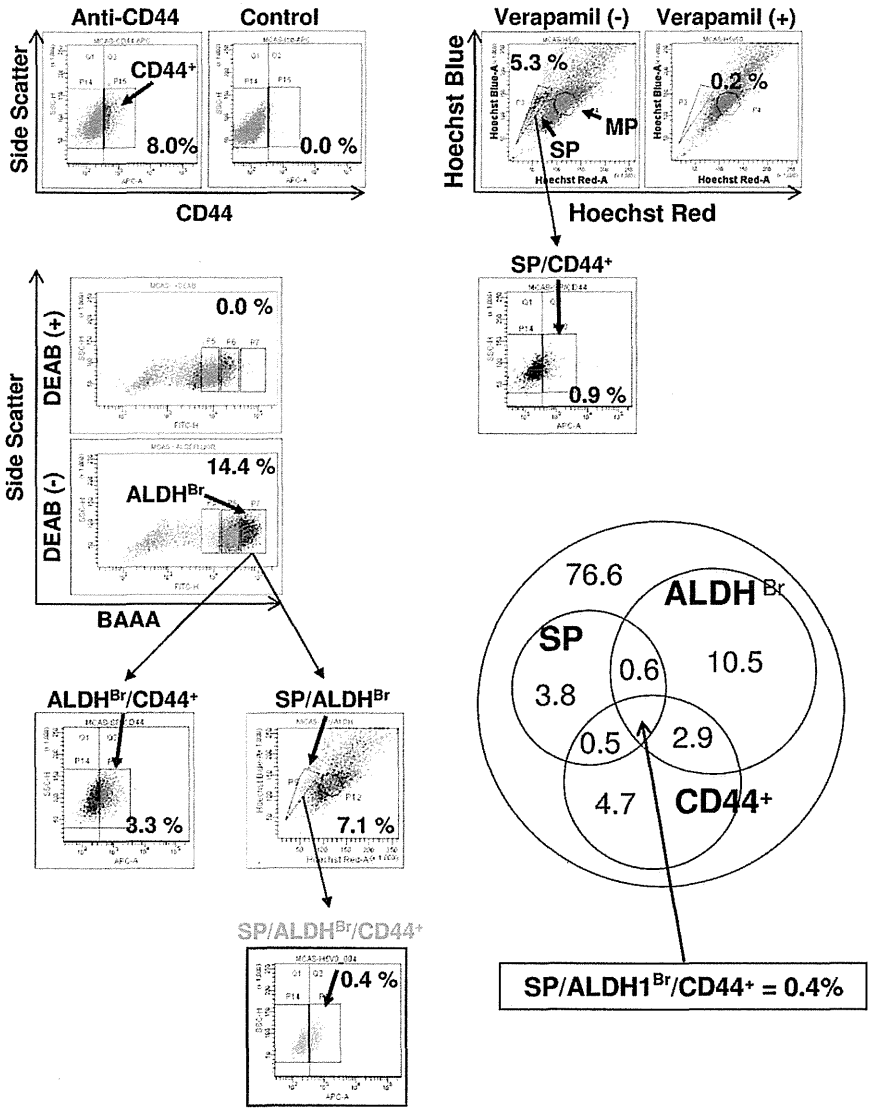

Figure 6. SP, ALDEFLUOR and CD44 triple staining. MCAS cells were stained by Hoechst 33342 dye, BAAA and anti-CD44 antibody, and analyzed. The ratios of SP, ALDH^{Br}, CD44^{+}, SP/ALDH^{Br}, SP/CD44^{+}, ALDH^{Br}/CD44^{+} and SP/ALDH^{Br}/CD44^{+} cells were 5.3%, 14.4%, 8.0%, 1.0%, 0.9%, 3.3% and 0.4%, respectively.
doi:10.1371/journal.pone.0068187.g006

Supporting Information

Figure S1 SP and ALDEFLUOR dual assay. OVCAR3, OVSAHO, HTBoA and HEC-1 cells were analyzed by SP and ALDEFLUOR dual assay. Percentages indicate the ratios of ALDH^{Br}, SP and SP/ALDH^{Br} cells.
(TIF)

Acknowledgments

The authors thank Ms. Eri Saka for technical assistance.

Author Contributions

Conceived and designed the experiments: KY TT YH NS. Performed the experiments: KY RM TK AT VK HA. Analyzed the data: KY TT YH NS. Contributed reagents/materials/analysis tools: KY TK JM TS TH. Wrote the paper: KY TT YH NS.

References

1. Rosen JM, Jordan CT (2009) The increasing complexity of the cancer stem cell paradigm. Science 324: 1670–1673.
2. Ghaffari S (2011) Cancer, stem cells and cancer stem cells: old ideas, new developments. F1000 Med Rep 3: 23.
3. Hirohashi Y, Torigoe T, Inoda S, Morita R, Kochin V, et al. (2012) Cytotoxic T lymphocytes: Sniping cancer stem cells. Oncoimmunology 1: 123–125.
4. Dean M, Fojo T, Bates S (2005) Tumour stem cells and drug resistance. Nat Rev Cancer 5: 275–284.

5. Rich JN (2007) Cancer stem cells in radiation resistance. Cancer Res 67: 8980–8984.
6. Tirino V, Desiderio V, Paino F, De Rosa A, Papaccio F, et al. (2012) Cancer stem cells in solid tumors: an overview and new approaches for their isolation and characterization. FASEB J.
7. Lehmann C, Jobs G, Thomas M, Burtscher H, Kubbies M (2012) Established breast cancer stem cell markers do not correlate with in vivo tumorigenicity of tumor-initiating cells. Int J Oncol 41: 1932–1942.
8. Shmelkov SV, Butler JM, Hooper AT, Hormigo A, Kushner J, et al. (2008) CD133 expression is not restricted to stem cells, and both CD133+ and CD133− metastatic colon cancer cells initiate tumors. J Clin Invest 118: 2111–2120.
9. Burkert J, Otto WR, Wright NA (2008) Side populations of gastrointestinal cancers are not enriched in stem cells. J Pathol 214: 564–573.
10. Pecorelli S, Favalli G, Zigliani L, Odicino F (2003) Cancer in women. Int J Gynaecol Obstet 82: 369–379.
11. Szotek PP, Pieretti-Vanmarcke R, Masiakos PT, Dinulescu DM, Connolly D, et al. (2006) Ovarian cancer side population defines cells with stem cell-like characteristics and Mullerian Inhibiting Substance responsiveness. Proc Natl Acad Sci U S A 103: 11154–11159.
12. Deng S, Yang X, Lassus H, Liang S, Kaur S, et al. (2010) Distinct expression levels and patterns of stem cell marker, aldehyde dehydrogenase isoform 1 (ALDH1), in human epithelial cancers. PLoS One 5: e10277.
13. Zhang S, Balch C, Chan MW, Lai HC, Matei D, et al. (2008) Identification and characterization of ovarian cancer-initiating cells from primary human tumors. Cancer Res 68: 4311–4320.
14. Friel AM, Sergent PA, Patnaude C, Szotek PP, Oliva E, et al. (2008) Functional analyses of the cancer stem cell-like properties of human endometrial tumor initiating cells. Cell Cycle 7: 242–249.
15. Goodell MA, Brose K, Paradis G, Conner AS, Mulligan RC (1996) Isolation and functional properties of murine hematopoietic stem cells that are replicating in vivo. J Exp Med 183: 1797–1806.
16. Inoda S, Hirohashi Y, Torigoe T, Morita R, Takahashi A, et al. (2011) Cytotoxic T lymphocytes efficiently recognize human colon cancer stem-like cells. Am J Pathol 178: 1805–1813.
17. Ginestier C, Hur MH, Charafe-Jauffret E, Monville F, Dutcher J, et al. (2007) ALDH1 is a marker of normal and malignant human mammary stem cells and a predictor of poor clinical outcome. Cell Stem Cell 1: 555–567.
18. Michifuri Y, Hirohashi Y, Torigoe T, Miyazaki A, Kobayashi J, et al. (2012) High expression of ALDH1 and SOX2 diffuse staining pattern of oral squamous cell carcinomas correlates to lymph node metastasis. Pathol Int 62: 684–689.
19. Billon N, Iannarelli P, Monteiro MC, Glavieux-Pardanaud C, Richardson WD, et al. (2007) The generation of adipocytes by the neural crest. Development 134: 2283–2292.
20. Nakatsugawa M, Hirohashi Y, Torigoe T, Asanuma H, Takahashi A, et al. (2009) Novel spliced form of a lens protein as a novel lung cancer antigen, Lengsin splicing variant 4. Cancer Sci 100: 1485–1493.
21. Vathipadiekal V, Saxena D, Mok SC, Hauschka PV, Ozbun L, et al. (2012) Identification of a potential ovarian cancer stem cell gene expression profile from advanced stage papillary serous ovarian cancer. PLoS One 7: e29079.
22. Hirohashi Y, Torigoe T, Inoda S, Takahashi A, Morita R, et al. (2010) Immune response against tumor antigens expressed on human cancer stem-like cells/tumor-initiating cells. Immunotherapy 2: 201–211.
23. Wang YC, Yo YT, Lee HY, Liao YP, Chao TK, et al. (2012) ALDH1-bright epithelial ovarian cancer cells are associated with CD44 expression, drug resistance, and poor clinical outcome. Am J Pathol 180: 1159–1169.
24. Pierre-Louis O, Clay D, Brunet de la Grange P, Blazsek I, Desterke C, et al. (2009) Dual SP/ALDH functionalities refine the human hematopoietic Lin-CD34+CD38− stem/progenitor cell compartment. Stem Cells 27: 2552–2562.
25. Varghese S, Whipple R, Martin SS, Alexander HR (2012) Multipotent cancer stem cells derived from human malignant peritoneal mesothelioma promote tumorigenesis. PLoS One 7: e52825.
26. Nakatsugawa M, Takahashi A, Hirohashi Y, Torigoe T, Inoda S, et al. (2011) SOX2 is overexpressed in stem-like cells of human lung adenocarcinoma and augments the tumorigenicity. Lab Invest 91: 1796–1804.
27. Shi MF, Jiao J, Lu WG, Ye F, Ma D, et al. (2010) Identification of cancer stem cell-like cells from human epithelial ovarian carcinoma cell line. Cell Mol Life Sci 67: 3915–3925.
28. Wang L, Mezencev R, Bowen NJ, Matyunina LV, McDonald JF (2012) Isolation and characterization of stem-like cells from a human ovarian cancer cell line. Mol Cell Biochem 363: 257–268.
29. Clevers H (2011) The cancer stem cell: premises, promises and challenges. Nat Med 17: 313–319.
30. Lapidot T, Sirard C, Vormoor J, Murdoch B, Hoang T, et al. (1994) A cell initiating human acute myeloid leukaemia after transplantation into SCID mice. Nature 367: 645–648.
31. Bonnet D, Dick JE (1997) Human acute myeloid leukemia is organized as a hierarchy that originates from a primitive hematopoietic cell. Nat Med 3: 730–737.
32. Al-Hajj M, Wicha MS, Benito-Hernandez A, Morrison SJ, Clarke MF (2003) Prospective identification of tumorigenic breast cancer cells. Proc Natl Acad Sci U S A 100: 3983–3988.
33. Huang EH, Hynes MJ, Zhang T, Ginestier C, Dontu G, et al. (2009) Aldehyde dehydrogenase 1 is a marker for normal and malignant human colonic stem cells (SC) and tracks SC overpopulation during colon tumorigenesis. Cancer Res 69: 3382–3389.
34. Wang R, Chadalavada K, Wilshire J, Kowalik U, Hovinga KE, et al. (2010) Glioblastoma stem-like cells give rise to tumour endothelium. Nature 468: 829–833.
35. Takahashi K, Yamanaka S (2006) Induction of pluripotent stem cells from mouse embryonic and adult fibroblast cultures by defined factors. Cell 126: 663–676.
36. Silva IA, Bai S, McLean K, Yang K, Griffith K, et al. (2011) Aldehyde dehydrogenase in combination with CD133 defines angiogenic ovarian cancer stem cells that portend poor patient survival. Cancer Res 71: 3991–4001.
37. Goodell MA, Rosenzweig M, Kim H, Marks DF, DeMaria M, et al. (1997) Dye efflux studies suggest that hematopoietic stem cells expressing low or undetectable levels of CD34 antigen exist in multiple species. Nat Med 3: 1337–1345.
38. Ma I, Allan AL (2011) The role of human aldehyde dehydrogenase in normal and cancer stem cells. Stem Cell Rev 7: 292–306.

ERAAP and Tapasin Independently Edit the Amino and Carboxyl Termini of MHC Class I Peptides

Takayuki Kanaseki,*,†,[1] Kristin Camfield Lind,*,[1] Hernando Escobar,‡ Niranjana Nagarajan,* Eduardo Reyes-Vargas,‡ Brant Rudd,‡ Alan L. Rockwood,‡ Luc Van Kaer,§ Noriyuki Sato,† Julio C. Delgado,‡ and Nilabh Shastri*

Effective CD8$^+$ T cell responses depend on presentation of a stable peptide repertoire by MHC class I (MHC I) molecules on the cell surface. The overall quality of peptide–MHC I complexes (pMHC I) is determined by poorly understood mechanisms that generate and load peptides with appropriate consensus motifs onto MHC I. In this article, we show that both tapasin (Tpn), a key component of the peptide loading complex, and the endoplasmic reticulum aminopeptidase associated with Ag processing (ERAAP) are quintessential editors of distinct structural features of the peptide repertoire. We carried out reciprocal immunization of wild-type mice with cells from Tpn- or ERAAP-deficient mice. Specificity analysis of T cell responses showed that absence of Tpn or ERAAP independently altered the peptide repertoire by causing loss as well as gain of new pMHC I. Changes in amino acid sequences of MHC-bound peptides revealed that ERAAP and Tpn, respectively, defined the characteristic amino and carboxy termini of canonical MHC I peptides. Thus, the optimal pMHC I repertoire is produced by two distinct peptide editing steps in the endoplasmic reticulum. ***The Journal of Immunology*****, 2013, 191: 1547–1555.**

Presentation of endogenous peptides by MHC class I (MHC I; peptide–MHC I complexes [pMHC I]) on the cell surface enables the immune system to detect and eliminate infected or transformed cells. The peptides are generated from intracellular proteins and loaded onto MHC I by the Ag processing pathway (1, 2). The pathway begins in the cytoplasm where antigenic precursors are fragmented to produce a pool of intermediate peptide fragments. The fragments are transported into the endoplasmic reticulum (ER) where they are loaded onto MHC I molecules. The resulting pMHC I are exported to the cell surface to serve as potential ligands for recognition by the CD8$^+$ T cell Ag receptors. Because circulating CD8$^+$ T cells make only transient contacts with APCs, effective CD8$^+$ T cell responses are critically dependent on presentation of an optimally stable pMHC I repertoire.

To elicit robust CD8$^+$ T cell responses, we selected peptides entering the Ag presentation pathway to yield high-affinity pMHC I that will persist on the cell surface. In addition to a characteristic length of 8–10 aa, the peptides presented by MHC I on the cell surface are uniquely defined by the presence of conserved consensus motifs. The set of peptides bound by a given MHC I molecule shares conserved amino acids located at discrete positions, called anchor residues, that allow peptide binding to the MHC I (3). Amino acid substitutions at these anchor positions resulted in loss of stable interactions between peptides and MHC I that, in turn, inhibited CD8$^+$ T cell responses.

The pool of peptides for MHC I presentation is produced from endogenously synthesized proteins fragmented mainly by the multicatalytic proteasome (4), as well as other proteases (5, 6). These models suggest that cytoplasmic proteolysis is primarily responsible for generating the canonical C termini of antigenic peptides. The intermediate peptide fragments are transported into the ER by the TAP (7). Upon entering the ER, the peptides encounter the peptide loading complex (PLC) that facilitates loading of optimal peptide onto MHC I (8, 9). The PLC consists of TAP, the chaperones tapasin (Tpn) and calreticulin, the thiol oxidoreductase ERp57, β_2-microglobulin, and the MHC I H chain. Among these components, Tpn is critical for the formation and function of the PLC (8–10). Tpn interacts directly with TAP, the MHC I H chain, and ERp57, thereby bringing the PLC components together and keeping the empty MHC I close to the source of incoming peptides (9–15). Consistent with its central function in the PLC, surface expression of MHC I molecules is profoundly diminished in Tpn-deficient mice (16, 17) and in several MHC I molecules in human cells (9, 18). Furthermore, the loss of Tpn results in presentation of suboptimal pMHC I (9, 11, 17, 19–22). Thus, Tpn is the key mediator of peptide loading in the PLC. Nevertheless, the molecular features of the peptide cargo affected by Tpn remain unknown.

The ER aminopeptidase associated with Ag processing (ERAAP) has emerged as yet another editor of the pMHC I repertoire in the ER (23, 24). The loss of ERAAP caused profound changes in the

*Division of Immunology and Pathogenesis, Department of Molecular and Cell Biology, University of California, Berkeley, Berkeley, CA 94720; †Department of Pathology, Sapporo Medical University, Sapporo, Hokkaido 060-8556, Japan; ‡ARUP Institute for Clinical and Experimental Pathology, Department of Pathology, University of Utah School of Medicine, Salt Lake City, UT 84108; and §Department of Pathology, Microbiology and Immunology, Vanderbilt University School of Medicine, Nashville, TN 37232

[1]T.K. and K.C.L. contributed equally to this work.

Received for publication April 23, 2013. Accepted for publication June 4, 2013.

This work was supported by the National Institutes of Health (N.S.).

Address correspondence and reprint requests to Dr. Nilabh Shastri, Division of Immunology, LSA 421, Department of Molecular and Cell Biology, University of California, Berkeley, Berkeley, CA 94720-3200. E-mail address: nshastri@berkeley.edu

The online version of this article contains supplemental material.

Abbreviations used in this article: BfA, brefeldin A; ER, endoplasmic reticulum; ERAAP, endoplasmic reticulum aminopeptidase associated with Ag processing; ERAAP$^{-/-}$TAP$^{-/-}$, ERAAP and TAP double-deficient; ERAAP$^{-/-}$Tpn$^{-/-}$, ERAAP and Tpn double-deficient; K^{b}D^b dko, K^b and D^b double-deficient; MHC I, MHC class I; PLC, peptide loading complex; pMHC I, peptide–MHC I complex; Tpn, tapasin; WT, wild-type.

www.jimmunol.org/cgi/doi/10.4049/jimmunol.1301043

pMHC I repertoire relative to wild-type (WT) mice (25–29). Analysis of $CD8^+$ T cell responses elicited in WT mice by ERAAP-deficient cells showed that classical as well as nonclassical MHC I presented a distinct, highly immunogenic peptide repertoire (26, 27, 30, 31). Furthermore, examination of the sequence of presented peptides in ERAAP-deficient cells by mass spectrometry revealed that the peptides were longer, often because of extra N-terminal residues (30). How ERAAP edits peptides presented by MHC I and whether editing occurs within the PLC is not known. Because Tpn physically brings together PLC components, cells without Tpn lack a functional PLC. We reasoned that the peptide editing events in the PLC might be evident in cells lacking Tpn or ERAAP.

In this study, we analyzed the peptide editing functions of Tpn and ERAAP required for generating the optimal pMHC I repertoire. We examined peptide editing events in cells lacking Tpn or ERAAP. By immunological, biochemical, and molecular analyses, we find that ERAAP and Tpn independently edited the N and C termini of the peptide repertoire presented by MHC I on the cell surface.

Materials and Methods

Mice

ERAAP-deficient (25), Tpn-deficient (16), TAP1-deficient (32), and K^b and D^b double-deficient (K^bD^b dko) mice (33) have been described elsewhere. C57BL/6J mice were purchased from The Jackson Laboratory. ERAAP- and Tpn-deficient mice were crossed to generate ERAAP and Tpn double-deficient ($ERAAP^{-/-}Tpn^{-/-}$) mice. Use of all mice was done with the approval of the Animal Care and Use Committee of the University of California at Berkeley.

Antibodies

The following Abs used for flow cytometry analysis were purchased from BD Biosciences: anti–H-$2K^b$ (AF6-88.5), anti–H-$2A^b$ (25-9-17), anti-CD8α (53-6.7), anti-CD4 (RM4-5), and anti–IFN-γ (XMG1.2). Abs CD16/32 (Fc block, clone 93) and anti–H-$2D^b$ (28-14-8) were purchased from eBiosciences. For in vivo depletions, purified anti-NK1.1 Ab (PK136) from BioXcell was used. To block presentation by MHC I to T cell lines, we used the following culture supernatants: anti–H-$2K^b$ (5F1.5), anti–H-$2D^b$ (B22.249), or anti–H-$2A^b$ (M5/114). In the immunoaffinity purification of pMHC I for mass spectrometry, anti–H-$2K^b$ (Y3) and anti–H-$2D^b$ (B22.249) were used.

Cell lines and DNA constructs

ERAAP and TAP double-deficient ($ERAAP^{-/-}TAP^{-/-}$) fibroblasts were previously reported, and immortalized $ERAAP^{-/-}Tpn^{-/-}$ fibroblast cell lines were generated in the same manner as previously described (25). The use and generation of β-galactosidase (lacZ)–inducible T cell hybridomas B3Z, 30NXZ, 1AZ, 11P9Z, LPAZ, 27.5Z, and BEKo8Z have been described elsewhere (25, 31). Activation of T cell hybridomas was determined by measurement of cleavage of the lacZ substrate chlorophenol red-β-D-galactopyranoside (Roche). Splenocytes from indicated mice treated with 200 ng/ml LPS (Sigma) for 14–16 h were used as APCs for T cell hybridomas. The ES-X9[SHL8] construct containing ER-localization sequence followed by N terminally extended antigenic SIINFEHL (SHL8) peptide was previously described (34).

Peptide extraction and reverse-phase HPLC analysis

The preparation, fractionation, and detection of the peptide extracts has been described previously (34). In brief, the peptides were eluted from the cells by 10% formic acid, fractionated by reverse-phase HPLC, treated with trypsin, and assayed as described previously. Synthetic peptides were prepared by D. King (University of California at Berkeley).

Immunizations and CTL lines

To generate T cell lines, we immunized female Tpn-deficient or WT mice i.p. with 2×10^7 spleen cells from male WT or Tpn-deficient mice, respectively. Ten days after immunization, spleen cells were restimulated in vitro. Cultures contained 20 U/ml (first two restimulations) or 50 U/ml (subsequent restimulations) hIL-2 (BD Biosciences) and irradiated spleen cells from female mice of the same genotype used for immunization. Additional restimulations were done every 7–10 d.

Measurement of intracellular IFN-γ production by CTLs

The $CD8^+$ T cell responses of the immunized mice were measured by assessment of intracellular IFN-γ production. Spleen cell APCs were treated with 200 ng/ml LPS (Sigma) overnight, and $CD4^+$ and $CD8^+$ cells were depleted using magnetic beads (Dynal Biotech, Invitrogen) before incubation with restimulated $CD8^+$ T cells. A total of 1 μl/ml brefeldin A (BfA; GolgiPlug [BD Biosciences]) was added after 1 h, and total incubation of $CD8^+$ T cells and APCs was 5 h. Cells were stained for surface markers followed by intracellular staining for IFN-γ. Cells were analyzed by flow cytometry using an LSR II (BD) and with FlowJo Software (TreeStar). All plots were first gated on live cells based on forward/side scatter, followed by gating on $CD8^+$ and IFN-γ^+. For blocking of particular MHC I molecules, APCs were first incubated for 30 min on ice with Ab supernatant before addition of $CD8^+$ T cells as described earlier. For analysis of pMHC I surface stability, APCs were incubated for 2 or 4 h at 37°C in medium containing 8 mg/ml BfA (Sigma) followed by addition of $CD8^+$ T cells and staining as described earlier.

In vivo cytotoxicity assay

WT female mice, depleted of NK cells at least 36 h before every immunization, were primed i.p. with 2×10^7 male WT, $ERAAP^{-/-}$, or $Tpn^{-/-}$ splenocytes. Mice were challenged on day 7 with a 1:1:1 mix of labeled $ERAAP^{-/-}$, $Tpn^{-/-}$, and WT female APCs. Target cell labels were $ERAAP^{-/-}$ labeled with 20 μM CellTracker Blue CMAC (7-amino-4-chloromethylcoumarin; Invitrogen), $Tpn^{-/-}$ targets labeled with 0.125 μM CFSE (low dose), and WT targets labeled with 1.25 μM CFSE (high dose; Invitrogen). Twenty hours after challenge with labeled cells, host mice were sacrificed and splenocytes analyzed by flow cytometry to determine percentage of cells remaining. Plots were gated on live cells before analysis of target populations. Percent specific lysis was calculated as follows: $100 \times (1 - [\text{ratio of target output}]/[\text{ratio of target input}])$, where input is determined before injection of targets and output represents targets recovered after challenge. To calculate ratios, (% population of interest)/(%$ERAAP^{-/-}$ + %$Tpn^{-/-}$ + %WT).

Large-scale peptide sequencing by tandem mass spectrometry

Peptide sequencing using immunoaffinity purification of pMHC complexes from detergent-solubilized spleen lysates was performed as reported previously (35). In brief, freshly isolated spleen cells from 25 C57BL/6 and 50 Tpn-deficient mice were lysed and pMHC I was immuno-purified using mAbs Y3 (anti–H-$2K^b$) and B22.249 (anti–H-$2D^b$). Samples were subject to fast protein liquid chromatography-HPLC fractionation, and sequence identification by nanochip electrospray ionization-quadrupole time of flight mass spectrometer. Peptides were identified with high confidence using an initial search with Spectrum Mill algorithm followed by expert manual spectral validation (36). To analyze the amino acid conservation of groups of more than seven peptides, we used WebLogo program (http://weblogo.berkeley.edu/).

Results

ERAAP and Tpn differentially influence pMHC I repertoire

ERAAP and Tpn are both ER-resident editors of the peptide repertoire presented by MHC I. To assess the relative contributions of ERAAP and Tpn to the overall peptide repertoire, we measured pMHC I surface expression by flow cytometry (Fig. 1A–C). Spleen cells from WT, $Tpn^{-/-}$, $ERAAP^{-/-}$, $ERAAP^{-/-}Tpn^{-/-}$, TAP-deficient ($TAP^{-/-}$), or K^bD^b dko strains were stained for D^b and K^b MHC I (Fig. 1A, 1B), as well as the MHC II molecule A^b as a negative control (Fig. 1C). Compared with WT C57BL/6 mice, loss of ERAAP diminished MHC expression by ~20%, whereas loss of Tpn with or without ERAAP expression diminished MHC expression by ~90% (16, 17, 34). However, Tpn-deficient cells expressed relatively more pMHC I compared with cells lacking TAP1, the peptide transporter, or cells completely lacking K^b, as well as D^b MHC I. Thus, ERAAP and especially Tpn were required for maintaining normal level of pMHC I expression on the cell surface.

We next assessed the influence of ERAAP and Tpn on the generation of specific peptides bound to MHC I. We measured the presentation of a panel of endogenously processed peptides on the surface of spleen cells from WT B6, Tpn-deficient ($Tpn^{-/-}$),

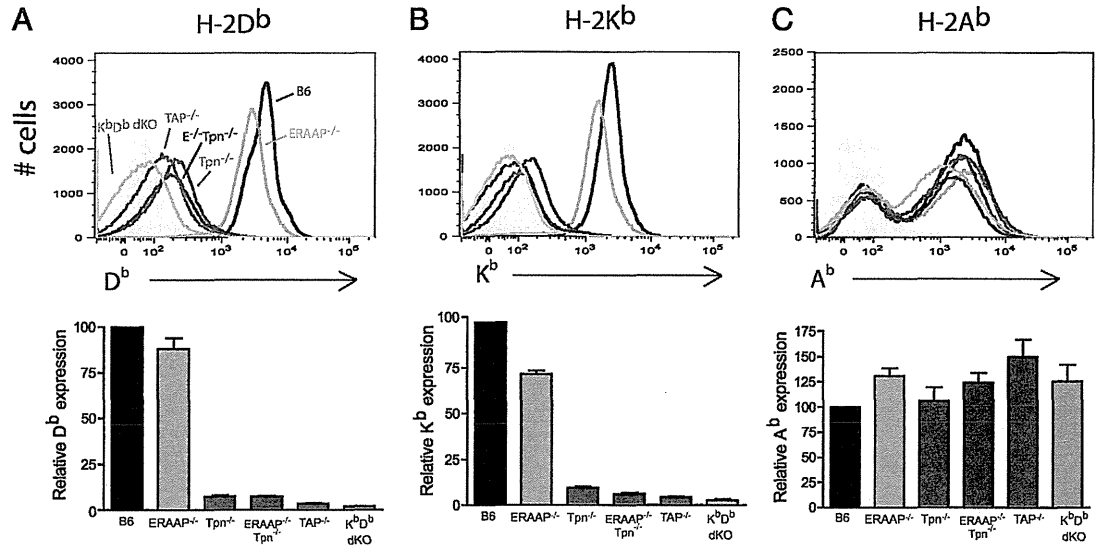

FIGURE 1. Tpn and ERAAP differentially affect surface pMHC I expression. (**A–C**) Surface (A) H-2D^b, (B) H-2K^b, and (C) H-2A^b expression on spleen cells derived from WT, ERAAP$^{-/-}$, Tpn$^{-/-}$, ERAAP$^{-/-}$Tpn$^{-/-}$, TAP$^{-/-}$, and K^{b}D^b dko mice. Bar graphs summarize the mean fluorescence intensity. FACS plots are gated on live cells. *Top panels* show representative data; *bottom panels* show data from three independent experiments.

or ERAAP-deficient (ERAAP$^{-/-}$) mice (Fig. 2). The absence of ERAAP affected pMHC I presentation differentially (23, 25, 31), ranging from no detectable change in the pK^b ligand recognized by the 27.5Z hybridoma to an almost complete loss of the pMHC I ligands recognized by the LPAZ and 11p9Z hybridomas. In contrast, presentation of pMHC I ligands recognized by 1AZ, 30NXZ, and BEko8Z hybridomas was markedly enhanced on surface of ERAAP-deficient cells. In contrast, loss of Tpn was generally deleterious for all the pMHC I ligands tested. Taken together, these observations show that normal expression of pMHC I was influenced by ERAAP and even more so by Tpn.

Absence of Tpn causes selective loss of pMHC I ligands

To further define the specific changes that occurred in the pMHC I repertoire because of loss of Tpn, we took advantage of the immune systems' ability to detect differences between self and nonself. If certain pMHC I were absent in Tpn-deficient mice, specific CD8$^+$ T cells would not be tolerized to them and would respond to the novel pMHC I expressed by WT cells. We immunized Tpn$^{-/-}$ mice with WT spleen cells expressing the normally diverse pMHC I repertoire. After 10 d, splenocytes from recipient mice were restimulated for a week with WT spleen cells. The cultures were then analyzed for presence of CD8$^+$ T cells that produced IFN-γ when stimulated with spleen cell APCs of the indicated genotype. The Tpn$^{-/-}$ anti-WT CD8$^+$ T cells responded strongly to WT APCs but not to self APCs (Fig. 3A, 3B), showing that Tpn-deficient mice perceived normal pMHC I as foreign in WT cells. We infer that Tpn deficiency caused the loss of many pMHC I normally present in WT cells. Typical of peptides presented by MHC I, these pMHC I required TAP for their presentation (Fig. 3B).

To establish the ligand specificity of the responding CD8$^+$ T cells, we used spleen cells from K^{b}D^b dko mice as APCs. The Tpn$^{-/-}$

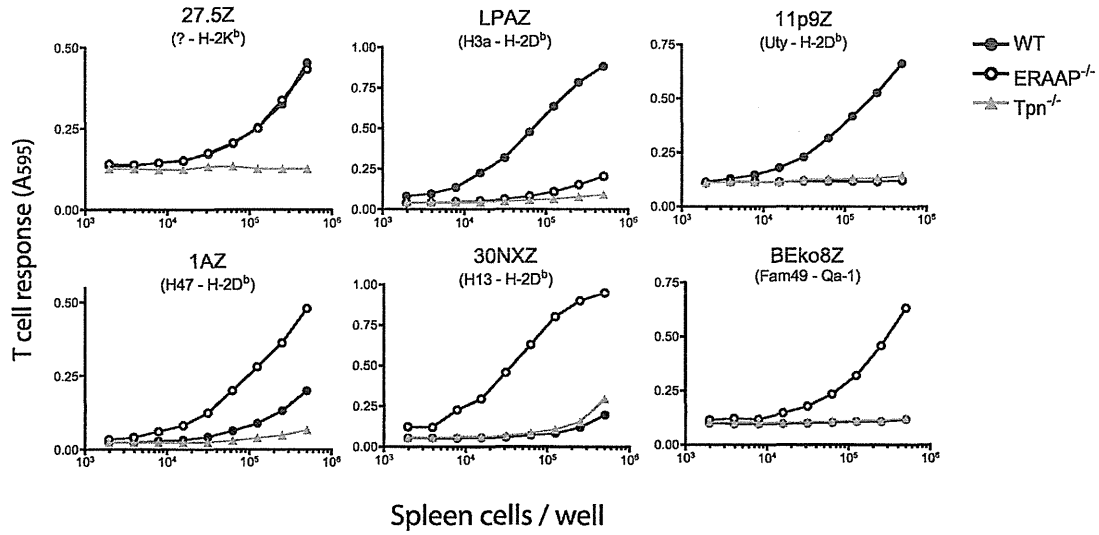

FIGURE 2. Tpn and ERAAP differentially affect presentation of endogenous pMHC I by spleen cells. Splenocytes from indicated male mice were stimulated with 200 ng/ml LPS overnight before incubation with CD8$^+$ T cell hybridomas 27.5Z, LPAZ, 11P9Z, 1AZ, 30NXZ, or BEKo8Z. Hybridomas specifically recognize peptides encoded by the indicated genes and presented on H-2D^b, H-2K^b, or Qa-1^b. Hybridoma response is determined by assessing conversion of the colorimetric substrate chlorophenol red-β-D-galactopyranoside to chlorophenol red measured at absorbance at 595 nm (A595). Data are representative of three independent experiments.

anti-WT T cells did not respond to K^bD^b dko spleen cells, indicating that Tpn-dependent peptides were presented by K^b and D^b MHC I in WT cells, rather than nonclassical MHC I molecules (Fig. 3B).

Tpn-deficient cells also express novel immunogenic pMHC I

To determine whether loss of Tpn editing also resulted in presentation of novel pMHC I, we immunized WT mice with $Tpn^{-/-}$ cells. The recipient T cells were restimulated in vitro and analyzed for responses to WT or $Tpn^{-/-}$ APCs. WT anti-$Tpn^{-/-}$ T cells produced IFN-γ in response to $Tpn^{-/-}$, but not to self WT APCs, indicating presence of novel pMHC I in $Tpn^{-/-}$ cells (Fig. 4A, 4B).

Tpn expression appears to affect TAP stability and could thus influence peptide transport into the ER (37). Therefore, it was possible that the peptides presented in the absence of Tpn could be independent of TAP transport (38, 39). However, when we used $TAP^{-/-}$ cells as APCs, WT anti-$Tpn^{-/-}$ T cells did not produce IFN-γ (Fig. 4B), indicating that peptide transport is required for presentation of these pMHC I, and that this presentation is not a consequence of TAP deficiency. Furthermore, although blocking the A^b MHC II molecule or the K^b MHC I molecule did not inhibit IFN-γ production in any of the five lines tested, blocking with the anti-D^b Ab inhibited T cell responses more effectively than blocking with anti-K^b (Fig. 4C). The possible contribution of $CD8^+$ T cells restricted by other nonclassical MHC I to the overall $CD8^+$ T cell response is presently unclear. Alternatively, some ligands may represent novel pMHC I conformations that are not recognized by conventional anti-MHC I Abs. Together, these results show that loss of Tpn not only caused a profound loss of pMHC I, it also allowed generation of new and immunologically distinct pMHC I.

In $Tpn^{-/-}$ mice, many K^b and D^b are less stable on the cell surface than in their WT counterparts (16). To test the stability of the immunogenic pMHC I in $Tpn^{-/-}$ cells, we used WT or $Tpn^{-/-}$ splenocytes as APCs after treatment with BfA, an inhibitor of ER-Golgi transport, for either 2 or 4 h (Fig. 4D). Although BfA treatment of WT APCs did not affect expression of pMHC I recognized by the $Tpn^{-/-}$ anti-WT T cells, treatment of $Tpn^{-/-}$ APCs caused a dramatic loss of WT–anti-$Tpn^{-/-}$–stimulating ligands. Thus, even though pMHC I expressed by $Tpn^{-/-}$ cells were markedly less stable than those expressed by WT cells, they were nevertheless highly immunogenic.

PLC components TAP and Tpn are not required for peptide trimming by ERAAP

The loss and gain of novel pMHC I in either Tpn or ERAAP-deficient cells suggested the function of these two editors may be linked. For example, peptide trimming could be more effective if ERAAP interacted with the PLC that could provide ERAAP with access to incoming peptides and empty MHC I. To directly assess the role of PLC in determining ERAAP function, we analyzed peptide processing in cells lacking the key PLC components TAP or Tpn (Fig. 5A, 5B). We transfected $ERAAP^{-/-}TAP^{-/-}$ or $ERAAP^{-/-}Tpn^{-/-}$ fibroblasts with N-terminally extended SHL8 precursors in the presence or absence of WT ERAAP. The peptides extracted from transfected cells were fractionated by HPLC to separate the untrimmed precursor from the trimmed peptide products. The HPLC fractions were assayed for presence of antigenic peptides containing SHL8 with or without the N-terminal extension using the SHL8/K^b-specific B3Z hybridoma as described earlier (34). In $ERAAP^{-/-}TAP^{-/-}$ cells without ERAAP (vector alone), the N-terminally extended precursor peptide was the predominant peptide species (Fig. 5A, *upper panel*). Upon coexpression of ERAAP, the precursor peptide was no longer detected, and two peaks corresponding to the precisely cleaved SHL8 octapeptide and the KSHL8 nonapeptides were found (Fig. 5A, *lower panel*). The SHL8 and KSHL8 peptides, respectively, represent the final products presented by the K^b and D^b MHC I present in these cells. Likewise, the same precursor and processed peptides were detected in presence or absence of ERAAP in Tpn-deficient cells (Fig. 5B). Thus, in the ER, ERAAP could trim antigenic precursors to their final products in the absence of TAP or Tpn. The results show directly that expression of either TAP or Tpn, and therefore an intact PLC, is not required for N-terminal trimming of antigenic precursors by ERAAP.

Tpn- and ERAAP-deficient cells express unique, nonoverlapping pMHC I

To further assess the relationship between peptide editing by ERAAP and Tpn, we examined the potential overlap between novel peptides generated in the absence of Tpn or ERAAP. T cell lines generated in WT mice by immunization with Tpn or ERAAP-deficient cells were tested for responses to various APCs. The $Tpn^{-/-}$ anti-WT $CD8^+$ T cell lines responded to both WT and $ERAAP^{-/-}$ APCs equally well, suggesting that both cells presented the unique pMHC I that were lost in $Tpn^{-/-}$ mice (Fig. 6A). In contrast, the WT anti-$Tpn^{-/-}$ lines recognized only Tpn-deficient cells but did not recognize either WT or $ERAAP^{-/-}$ cells (Fig. 6B). Likewise, WT anti-$ERAAP^{-/-}$ lines recognized $ERAAP^{-/-}$ APCs but did not respond to either WT or $Tpn^{-/-}$ APCs (Fig. 6C). The lack of cross-reactivity between T cells specific for $Tpn^{-/-}$ or $ERAAP^{-/-}$ APCs showed that ERAAP and Tpn have distinct and nonoverlapping roles in editing peptides for presentation on MHC I.

To further rigorously establish the distinction between the immunologically distinct Tpn or ERAAP-dependent ligands, we

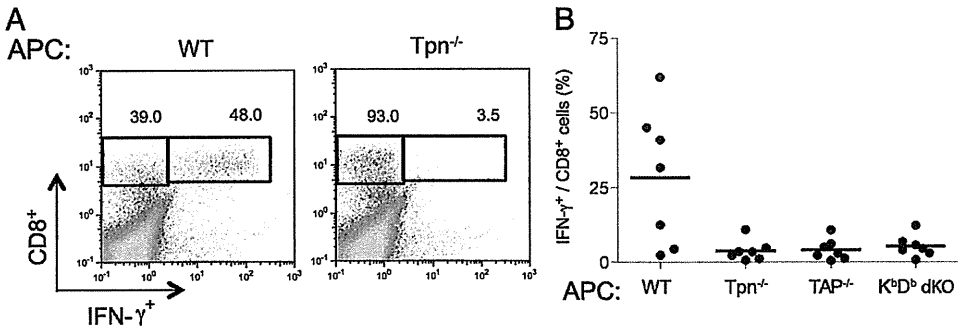

FIGURE 3. Tpn-deficient mice elicit $CD8^+$ T cell response to pMHC I expressed by WT cells. **(A)** Intracellular IFN-γ^+ produced by $Tpn^{-/-}$ anti-WT $CD8^+$ T cell lines in response to WT or $Tpn^{-/-}$ APCs. **(B)** $Tpn^{-/-}$ anti-WT $CD8^+$ T cell IFN-γ^+ response against WT, $Tpn^{-/-}$, $TAP^{-/-}$, or K^bD^b dko APCs. Each point represents an individual mouse. Data are from one of two independent experiments (A) or pooled from two independent experiments (B). (A and B) Numbers indicate percent IFN-γ^+ cells in the $CD8^+$ T cell gate.

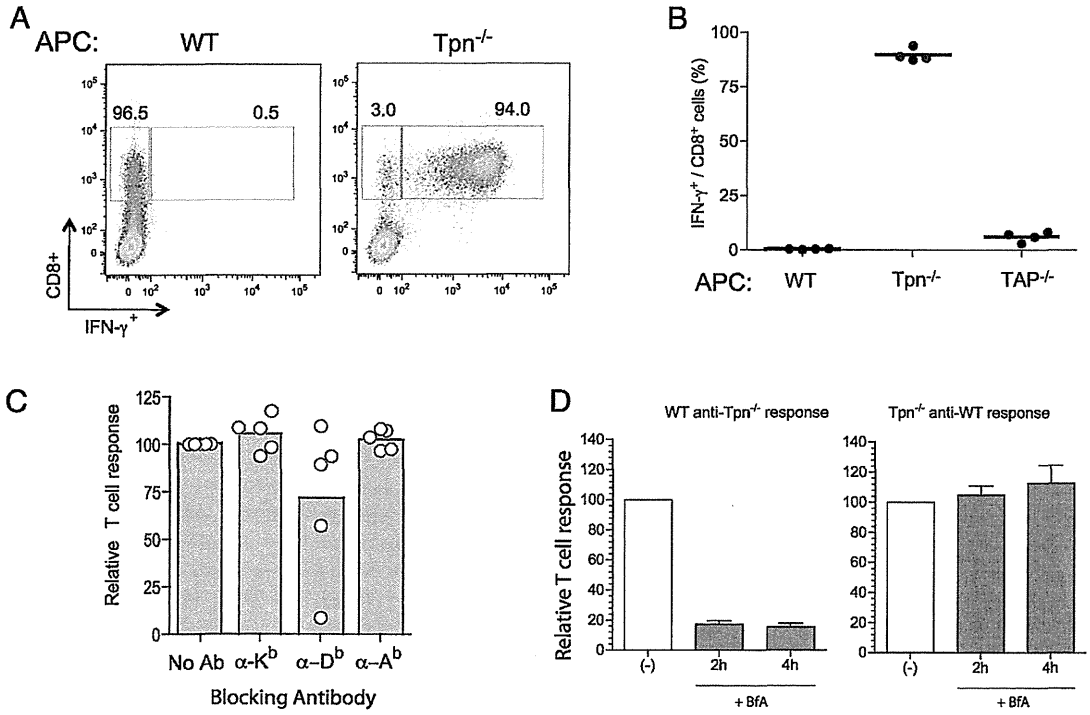

FIGURE 4. Tpn-deficient cells elicit $CD8^+$ T cell responses in WT mice. (**A**) IFN-γ^+ response of WT anti-$Tpn^{-/-}$ $CD8^+$ T cell lines against WT or $Tpn^{-/-}$ APCs. Numbers indicate percent IFN-γ^+ cells of total $CD8^+$ T cells. (**B**) WT anti-$Tpn^{-/-}$ $CD8^+$ T cell responses against WT, $Tpn^{-/-}$, or $TAP^{-/-}$ APCs. (A and B) Numbers indicate percent IFN-γ^+ cells in the $CD8^+$ T cell gate. (**C**) WT anti-$Tpn^{-/-}$ $CD8^+$ T cell responses against WT APCs previously treated with blocking Abs to MHC I K^b (α-K^b) or D^b (α-D^b), or to MHC II A^b (α-A^b). Percentages of $CD8^+$IFN-γ^+ cells were normalized to no Ab control (No Ab). (**D**) IFN-γ^+ production by WT anti-$Tpn^{-/-}$ (*left*) and $Tpn^{-/-}$ anti-WT (*right*) $CD8^+$ T cell lines against splenocyte APCs treated with BfA for 2 or 4 h before coculture with T cells. Percent of $CD8^+$ IFN-γ^+ was normalized to untreated (−). Data are representative of three independent experiments (A, B) or are pooled from two independent experiments (C, D).

assessed the ability of WT mice to eliminate $ERAAP^{-/-}$ or $Tpn^{-/-}$ target cells in vivo (Fig. 7). We primed WT mice with splenocytes from $ERAAP^{-/-}$, $Tpn^{-/-}$, or WT mice as a negative control. Seven days later, the mice were challenged with a cell mixture containing an equal number of WT, $ERAAP^{-/-}$, and $Tpn^{-/-}$ spleen cells as targets (Fig. 7A, 7B). We depleted NK cells in host mice before immunization and challenge to obviate the possible effect of these cells in targeting $Tpn^{-/-}$ or $ERAAP^{-/-}$ cells with lower MHC I expression (17, 40). To distinguish the three populations of donor cells recovered from host animals in vivo, we labeled each target cell population with a different fluorescent dye as shown schematically (Fig. 7A). After 20 h, spleens from host WT mice were analyzed for the presence of each labeled cell population (Fig. 7B, output). A decrease in the percentage of cells recovered relative to the WT (self) targets indicates elimination of individual populations by the immune system of WT hosts.

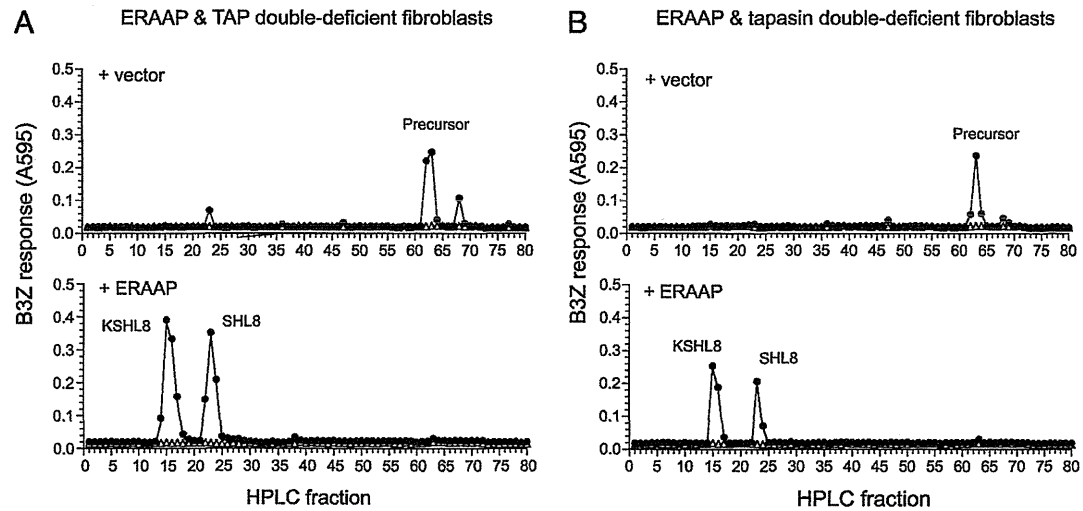

FIGURE 5. Peptide trimming by ERAAP does not require Tpn or TAP. (**A** and **B**) The ES-X9[SHL8] construct was cotransfected with ERAAP cDNA or with empty vector into (A) $ERAAP^{-/-}TAP^{-/-}$ or (B) $ERAAP^{-/-}Tpn^{-/-}$ fibroblasts. Cell lysates were fractionated by RP-HPLC and trypsinized to release SHL8 peptides before detection with B3Z hybridoma in the presence of L cells expressing H-$2K^b$. Synthetic SHL8 and KSHL8 peptide run under identical conditions verified the HPLC fraction numbers. Data are representative of three independent experiments.

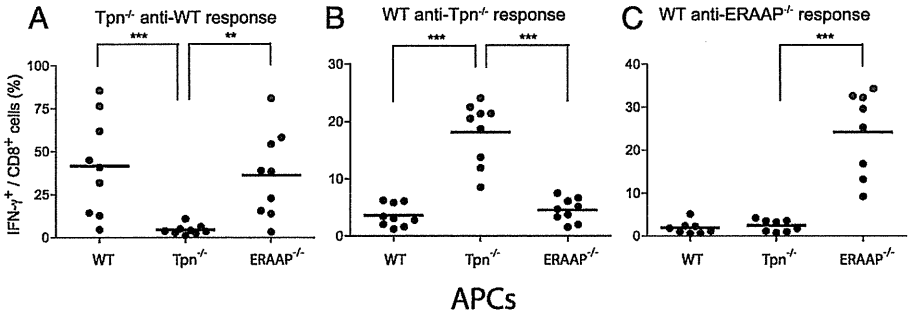

FIGURE 6. Immunogenic pMHC I expressed by Tpn or ERAAP-deficient cells do not overlap. T cell responses against indicated splenocyte APCs. (**A**) $Tpn^{-/-}$ anti-WT T cell response, (**B**) WT anti-$Tpn^{-/-}$ T cell response, and (**C**) WT anti-$ERAAP^{-/-}$ T cell response against spleen cell APCs derived from WT, $Tpn^{-/-}$, or $ERAAP^{-/-}$ mice. Immunizations to induce specific $CD8^+$ T cells and intracellular cytokine staining to detect IFN-γ production are described earlier. The p values were calculated by Mann–Whitney U test. $^{**}p < 0.01$, $^{***}p < 0.001$. Data are pooled from two (C) or three (A, B) independent experiments.

Mice primed with $ERAAP^{-/-}$ cells efficiently eliminated $ERAAP^{-/-}$ targets but did not influence the recovery of Tpn-deficient or self-WT cells (Fig. 7C). In contrast, WT mice primed with $Tpn^{-/-}$ splenocytes eliminated $Tpn^{-/-}$ targets, but not $ERAAP^{-/-}$ or WT targets. Finally, there was no specific loss of any of these target cells in mice primed with self-WT cells. Furthermore, the requirement for prior immunization for the in vivo elimination of $ERAAP^{-/-}$ or $Tpn^{-/-}$ targets suggests that these responses are mediated by the adaptive immune system. The in vitro and in vivo assessment of WT anti-$Tpn^{-/-}$ and WT-anti $ERAAP^{-/-}$ T cell lines demonstrates that the unedited peptide repertoires in cells deficient in ERAAP versus Tpn were distinct without any detectable overlap.

Tpn-deficient cells present peptides lacking canonical consensus motif

The earlier findings showed that loss of Tpn results in the presentation of a novel set of peptides on the cell surface that are immunogenic to WT T cells and are distinct from the unedited peptides presented by ERAAP-deficient cells. Our previous analysis of the unedited peptides in $ERAAP^{-/-}$ spleen cells had found that the novel peptides were longer in length and varied at their N termini (30). Whether specific structural changes also occurred in peptides produced in absence of Tpn is not known. To define the Tpn-dependent changes in the peptide repertoire, we isolated K^b and D^b pMHC I from WT as well as $Tpn^{-/-}$ splenocytes, eluted the bound peptides, and determined their amino acid sequences by tandem mass spectrometry. From WT cells, we identified 210 and 163 peptides bound to D^b and K^b, respectively. In contrast, the lower pMHC I expression in Tpn-deficient cells allowed recovery of fewer peptides; 63 and 22 peptides bound to D^b and K^b, respectively. We did not find any obvious differences in the intracellular localization of the source proteins for these peptides (data not shown). Many peptides in $Tpn^{-/-}$-deficient splenocytes were also found in WT mice (Fig. 8A, Supplemental Fig. 1A, Supplemental Tables I, II). Remarkably, comparison of the unique

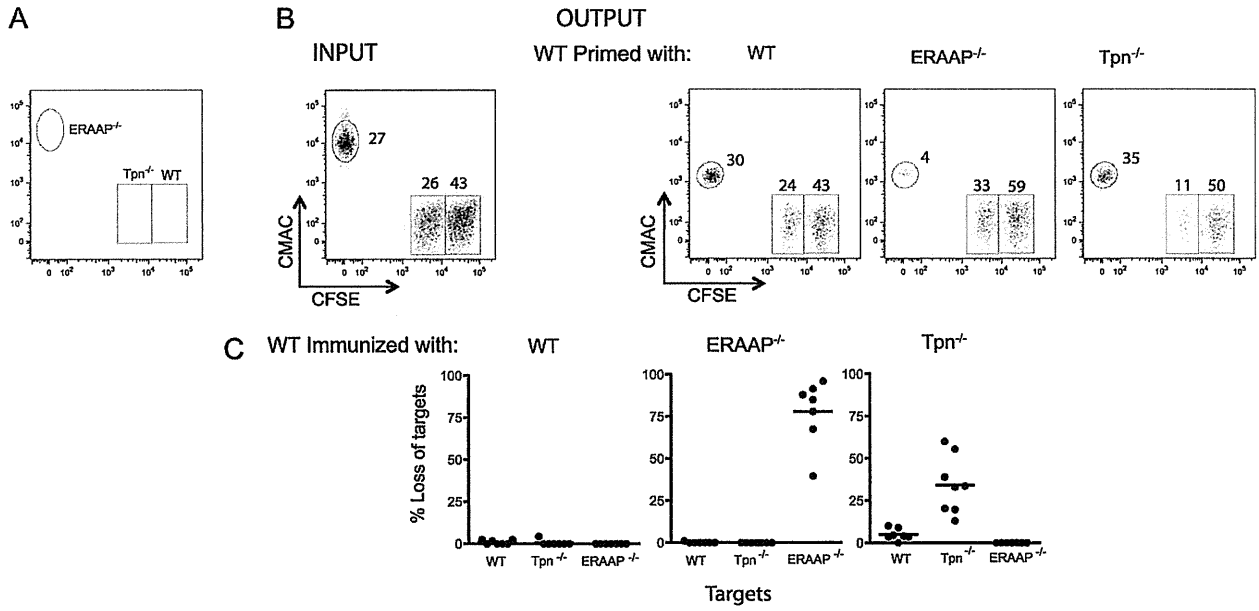

FIGURE 7. Different ligands are used for rejection of Tpn- or ERAAP-deficient cells by WT mice in vivo. T cells from WT mice primed 7 d earlier with male WT, $Tpn^{-/-}$, or $ERAAP^{-/-}$ splenocytes were assessed for their ability to specifically eliminate WT, $Tpn^{-/-}$, or $ERAAP^{-/-}$ female targets in vivo. Targets were given distinct labels so they could be compared in the same host mouse: WT = CFSE (high dose); $Tpn^{-/-}$ = CFSE (low dose); $ERAAP^{-/-}$ = CMAC. (**A**) Schematic indicating the populations that represent $ERAAP^{-/-}$, $Tpn^{-/-}$, and WT. (**B**) Representative FACS plots of labeled targets before (input) and after (output) challenge. Input refers to proportions of each labeled cell type before challenge, whereas output refers to the labeled populations identified 20 h posttransfer. (**C**) Summary of in vivo killing assay from (B). Negative loss (gain) is plotted as zero. Data are representative of two independent experiments (B) or are pooled from two independent experiments (C).

peptides in Tpn$^{-/-}$ cells with their WT counterparts revealed significant differences. First, peptides in Tpn$^{-/-}$ cells were markedly longer than those in WT cells (Fig. 8B, Supplemental Fig. 1B). Second, the canonical asparagine (N) residue at the p5 position of D^b bound peptides was consistently absent in peptides produced in absence of Tpn (Fig. 8C, 8D). A loss of the conserved phenylalanine or tyrosine residues (F/Y) at the p5 anchor position was less obvious in peptides bound to K^b (Supplemental Fig. 1C, 1D).

The most striking difference in the amino acid sequences was found in the C-terminal (PΩ) position of K^b and D^b peptides eluted from Tpn$^{-/-}$ samples. Typically, the C-terminal position is occupied by an aliphatic amino acid: Met (M), Ile (I), Leu (L), or Val (V), as seen in peptides found in WT cells (Fig. 8C, 8D, Supplemental Fig. 1C, 1D). However, in the Tpn$^{-/-}$ samples, a higher frequency of abnormal amino acids was identified at PΩ. These included Lys (K), Ser (S), Asn (N), Pro (P), and Ala (A) for D^b (Fig. 8C, 8D), and Thr (T) and Pro (P) for K^b (Supplemental Fig. 1C, 1D). Thus, the ability to choose the appropriate C-terminal amino acid, a key determinant of pMHC I stability, was lost in the absence of Tpn.

We verified the MHC I binding characteristics of a few representative peptides by assessing their ability to stabilize D^b or K^b on the surface of TAP-deficient RMA/s cells. Each peptide bound to the respective MHC I, although the binding was lower and the decay was faster than the canonical K^b and D^b binding peptides (Supplemental Fig. 2A–D). From Tpn-deficient mice, even the peptides that contained both anchor residues, such as FSPLNPVRV (D^b) and SLNRFIPL (K^b), were suboptimal binders of MHC I. Thus, in contrast with the striking influence of ERAAP on the N termini, Tpn primarily influenced the C-termini peptides presented by MHC I.

Discussion

We show in this article that generation of the optimal pMHC I repertoire required independent editing by Tpn and ERAAP. The absence of Tpn profoundly altered the pMHC I repertoire, causing loss of many pMHC I normally expressed in WT cells, as well as gain of other novel pMHC I. Interestingly, the new pMHC I in Tpn$^{-/-}$ cells were immunologically distinct from those found in cells lacking the N-terminal peptide editor, ERAAP. The CD8$^+$ T cells in WT mice elicited by either ERAAP$^{-/-}$ or Tpn$^{-/-}$ cells were highly specific and did not cross-react. Amino acid sequences of unedited peptides revealed that differences between the peptides in ERAAP versus Tpn-deficient cells were in their N- and C-terminal anchor residues, respectively. Thus, Tpn defines the C terminus, whereas ERAAP shapes the N terminus of canonical MHC I peptides.

The MHC I molecules present an extraordinarily diverse set of peptides to allow effective immune surveillance of virtually all endogenous proteins (3). Nevertheless, the canonical peptides presented by a given MHC I molecule share certain key features: a length of 8–10 aa, and the presence of conserved residues at the C terminus and at an internal p2 or p5 position (41). These conserved amino acids are called anchor residues because their presence determines the stability of the pMHC I (42). Editing of the available peptide repertoire is crucial to ensure that only the stable pMHC I reach the surface that are capable of triggering CD8$^+$ T cell responses. To generate the optimal pMHC I repertoire thus requires the editing mechanisms to determine the appropriate C termini, the length, as well as the internal conserved residues. The extent to which these choices are determined by the shape of the peptide binding groove of the MHC I itself versus other key players in the pathway has remained unclear.

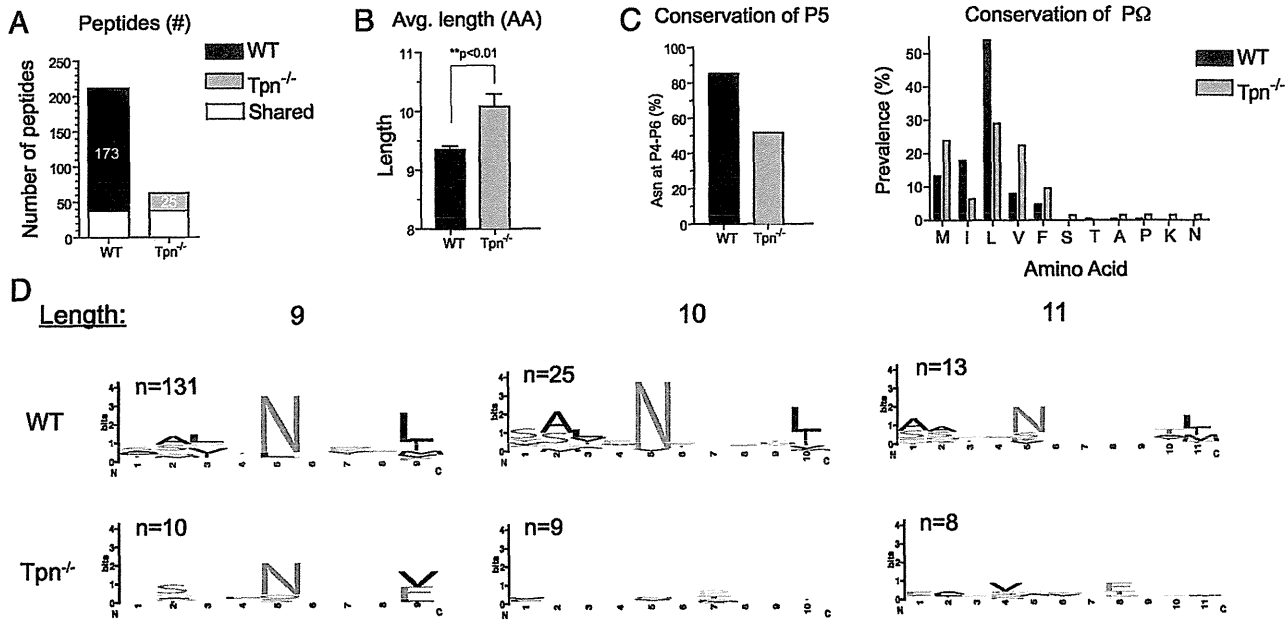

FIGURE 8. MHC I in WT and Tpn-deficient cells present unique peptides. The H-2D^b MHC I were immunoprecipitated from WT and Tpn-deficient spleen cells. Eluted peptides were sequenced by mass spectrometry and manually validated. (**A**) Numbers of distinct or shared peptides found in pMHC I expressed by WT or Tpn-deficient cells. (**B–D**) Analysis of the unique peptides from WT and Tpn-deficient cells. (B) The average lengths of peptides recovered from WT or Tpn-deficient cells. The indicated p value was calculated by two-tailed t test. (C) Conservation of p5 and C-terminal anchor residues (PΩ). Plots represent frequency of Asn (N) at P4–6 or the frequency of indicated amino acids at PΩ of H-2D^b peptides. (D) Logo representation of H-2D^b peptides eluted from WT or Tpn-deficient cells. Peptides are grouped according to their lengths, and the numbers of peptides in each group are indicated. The height of each bar is proportional to the degree of amino acid conservation, and the height of each letter composing the column is proportional to its frequency at the given position. Amino acids are colored as follows: hydrophobic (black), aromatic (purple), acidic (red), basic (blue), neutral (green), and the others (orange).

The MHC I molecules are loaded with their peptide cargo in the ER within the PLC (8). The crucial role of the PLC in peptide loading has been demonstrated by the severe loss of peptide-loaded MHC in cells without Tpn (16, 17). Tpn is the key element that holds the PLC together and retains the MHC I molecules in the ER until loaded with appropriate peptides (43). When various antigenic peptides were assessed for binding MHC I in the ER and subsequent display on the cell surface, presentation efficiency was determined by peptide affinity in presence of Tpn, but not other PLC components (20). Likewise, through in vitro reconstitution in microsomes, Tpn mediated the binding of high-affinity peptide to MHC I (44). Taken together with the severe reduction of pMHC I expression on the surface when Tpn was lost, these observations suggest that most peptides require editing in the PLC. Which structural aspects of the canonical MHC I–bound peptides determined the appropriate affinity threshold remained unclear.

We first used an immunological approach to characterize the changes in the peptide repertoire caused by loss of Tpn. We elicited $CD8^+$ T cell responses in WT mice immunized with spleen cells from Tpn-deficient mice and vice versa. Because the immune response has evolved to distinguish nonself from self, the $CD8^+$ T cell responses are exquisitely specific for nonself pMHC I. Importantly, the T cell can reveal changes in the pMHC I repertoire caused by alterations in Tpn expression that are not readily detected by any other assay. The specificity of the $CD8^+$ T cell responses showed that the absence of Tpn, like that of ERAAP described earlier (26), caused the loss of many WT pMHC I, as well as gain of other immunogenic pMHC I. As in ERAAP-deficient cells, the new pMHC I expressed by Tpn-deficient cells were also less stable, suggesting that the presented peptides were structurally distinct from their WT counterparts.

Interestingly, different structural changes in the pMHC I repertoire were caused by the loss of Tpn rather than by loss of ERAAP. We compared the effects of ERAAP versus Tpn deficiency to determine whether there were similarities in their editing functions. To examine a broad set of endogenous pMHC I, we compared the potential cross-reactivity of WT $CD8^+$ T cells responses elicited by Tpn versus ERAAP-deficient cells. We did not detect cross-reactivity between the two groups, suggesting that the unedited peptide repertoires of ERAAP−/− and Tpn−/− cells did not overlap. The lack of overlap between pMHC I generated in absence of ERAAP or Tpn was also found in vivo, ruling out potential artifacts caused by in vitro cultures. Although both ERAAP−/− and Tpn−/− unedited pMHC I were potently immunogenic and caused in vivo rejection, mice primed with Tpn−/− did not reject ERAAP−/− targets and vice versa. Independent analysis of naturally processed peptides extracted from living cells further confirmed that ERAAP function did not require Tpn or the peptide transporter, TAP. Together, these results strongly support the notion that Tpn and ERAAP edit different aspects of the pMHC I repertoire.

Mass spectrometry analysis of peptides eluted from ERAAP and Tpn-deficient spleen cells revealed the molecular basis for the structural differences in the unedited pMHC I repertoires. In the absence of Tpn, the most striking changes occurred at the C terminus where noncanonical amino acids at PΩ were far more frequent than in WT cells. In contrast, many more K^b and D^b bound peptides in ERAAP-deficient splenocytes were extended by extra amino acids at the N terminus or by potential bulges between the anchor residues, but the C termini always contained the canonical residues (30). Appropriate C-terminal anchor residues could therefore be maintained in presence of Tpn in ERAAP-deficient cells, but generation of the appropriate N termini required ERAAP. Thus, Tpn was important not only for integrity of the PLC, but also for its unique role in editing the C termini of peptides presented by MHC I.

Previous studies have assumed that cytosolic enzymes, such as the proteasome, generated peptides with canonical C-terminal residues (4, 45). However, our data showed that Tpn is the ultimate arbitrator for ensuring that peptides with appropriate C-terminal residue are presented. Consistent with a role for Tpn-mediated editing at the C termini of peptides, T134K mutation in the α2 helix of MHC I was found to affect Tpn–MHC I interactions in human cells (46). Although the molecular mechanism by which Tpn edits peptides is still unclear, putative models for peptide optimization via Tpn include accelerated dissociation of unfavorable peptides (40, 44, 47) or maintenance of the MHC I in a peptide-receptive conformation until bound by a high-affinity peptide (48). Notably, Tpn–MHC interactions occurred with the C-terminal end of the MHC I peptide binding groove.

In conclusion, Tpn and ERAAP edit distinct aspects of the peptides loaded onto MHC I molecules in the ER and explain the canonical features of the MHC I peptide cargo. Because the changes in pMHC I ligands due to failure of these editing steps are non-overlapping, it should be interesting to determine why Tpn or ERAAP are differentially targeted for immune evasion by viruses (49–51) and in cancer (40, 52).

Acknowledgments

We thank David King for peptide synthesis and Hector Nolla for assistance with flow cytometry.

Disclosures

The authors have no financial conflicts of interest.

References

1. Shastri, N., S. Cardinaud, S. R. Schwab, T. Serwold, and J. Kunisawa. 2005. All the peptides that fit: the beginning, the middle, and the end of the MHC class I antigen-processing pathway. *Immunol. Rev.* 207: 31–41.
2. Cresswell, P. 2005. Antigen processing and presentation. *Immunol. Rev.* 207: 5–7.
3. Rammensee, H.-G., K. Falk, and O. Rötzschke. 1993. Peptides naturally presented by MHC class I molecules. *Annu. Rev. Immunol.* 11: 213–244.
4. Rock, K. L., and A. L. Goldberg. 1999. Degradation of cell proteins and the generation of MHC class I-presented peptides. *Annu. Rev. Immunol.* 17: 739–779.
5. Reits, E., J. Neijssen, C. Herberts, W. Benckhuijsen, L. Janssen, J. W. Drijfhout, and J. Neefjes. 2004. A major role for TPPII in trimming proteasomal degradation products for MHC class I antigen presentation. *Immunity* 20: 495–506.
6. Kessler, J. H., S. Khan, U. Seifert, S. Le Gall, K. M. Chow, A. Paschen, S. A. Bres-Vloemans, A. de Ru, N. van Montfoort, K. L. Franken, et al. 2011. Antigen processing by nardilysin and thimet oligopeptidase generates cytotoxic T cell epitopes. *Nat. Immunol.* 12: 45–53.
7. Pamer, E. G., and P. Cresswell. 1998. Mechanisms of MHC class I—restricted antigen processing. *Annu. Rev. Immunol.* 16: 323–358.
8. Elliott, T., and A. Williams. 2005. The optimization of peptide cargo bound to MHC class I molecules by the peptide-loading complex. *Immunol. Rev.* 207: 89–99.
9. Ortmann, B., J. Copeman, P. J. Lehner, B. Sadasivan, J. A. Herberg, A. G. Grandea, S. R. Riddell, R. Tampé, T. Spies, J. Trowsdale, and P. Cresswell. 1997. A critical role for tapasin in the assembly and function of multimeric MHC class I-TAP complexes. *Science* 277: 1306–1309.
10. Tan, P., H. Kropshofer, O. Mandelboim, N. Bulbuc, G. J. Hämmerling, and F. Momburg. 2002. Recruitment of MHC class I molecules by tapasin into the transporter associated with antigen processing-associated complex is essential for optimal peptide loading. *J. Immunol.* 168: 1950–1960.
11. Dick, T. P., N. Bangia, D. R. Peaper, and P. Cresswell. 2002. Disulfide bond isomerization and the assembly of MHC class I-peptide complexes. *Immunity* 16: 87–98.
12. Peaper, D. R., P. A. Wearsch, and P. Cresswell. 2005. Tapasin and ERp57 form a stable disulfide-linked dimer within the MHC class I peptide-loading complex. *EMBO J.* 24: 3613–3623.
13. Bangia, N., P. J. Lehner, E. A. Hughes, M. Surman, and P. Cresswell. 1999. The N-terminal region of tapasin is required to stabilize the MHC class I loading complex. *Eur. J. Immunol.* 29: 1858–1870.
14. Simone, L. C., C. J. Georgesen, P. D. Simone, X. Wang, and J. C. Solheim. 2012. Productive association between MHC class I and tapasin requires the tapasin transmembrane/cytosolic region and the tapasin C-terminal Ig-like domain. *Mol. Immunol.* 49: 628–639.
15. Dong, G., P. A. Wearsch, D. R. Peaper, P. Cresswell, and K. M. Reinisch. 2009. Insights into MHC class I peptide loading from the structure of the tapasin-ERp57 thiol oxidoreductase heterodimer. *Immunity* 30: 21–32.

16. Grandea, A. G., III, T. N. Golovina, S. E. Hamilton, V. Sriram, T. Spies, R. R. Brutkiewicz, J. T. Harty, L. C. Eisenlohr, and L. Van Kaer. 2000. Impaired assembly yet normal trafficking of MHC class I molecules in Tapasin mutant mice. *Immunity* 13: 213–222.
17. Garbi, N., P. Tan, A. D. Diehl, B. J. Chambers, H.-G. Ljunggren, F. Momburg, and G. J. Hämmerling. 2000. Impaired immune responses and altered peptide repertoire in tapasin-deficient mice. *Nat. Immunol.* 1: 234–238.
18. Peh, C. A., S. R. Burrows, M. Barnden, R. Khanna, P. Cresswell, D. J. Moss, and J. McCluskey. 1998. HLA-B27-restricted antigen presentation in the absence of tapasin reveals polymorphism in mechanisms of HLA class I peptide loading. *Immunity* 8: 531–542.
19. Zarling, A. L., C. J. Luckey, J. A. Marto, F. M. White, C. J. Brame, A. M. Evans, P. J. Lehner, P. Cresswell, J. Shabanowitz, D. F. Hunt, and V. H. Engelhard. 2003. Tapasin is a facilitator, not an editor, of class I MHC peptide binding. *J. Immunol.* 171: 5287–5295.
20. Howarth, M., A. Williams, A. B. Tolstrup, and T. Elliott. 2004. Tapasin enhances MHC class I peptide presentation according to peptide half-life. *Proc. Natl. Acad. Sci. USA* 101: 11737–11742.
21. Park, B., and K. Ahn. 2003. An essential function of tapasin in quality control of HLA-G molecules. *J. Biol. Chem.* 278: 14337–14345.
22. Boulanger, D. S., R. Oliveira, L. Ayers, S. H. Prior, E. James, A. P. Williams, and T. Elliott. 2010. Absence of tapasin alters immunodominance against a lymphocytic choriomeningitis virus polytope. *J. Immunol.* 184: 73–83.
23. Serwold, T., F. Gonzalez, J. Kim, R. Jacob, and N. Shastri. 2002. ERAAP customizes peptides for MHC class I molecules in the endoplasmic reticulum. *Nature* 419: 480–483.
24. York, I. A., S. C. Chang, T. Saric, J. A. Keys, J. M. Favreau, A. L. Goldberg, and K. L. Rock. 2002. The ER aminopeptidase ERAP1 enhances or limits antigen presentation by trimming epitopes to 8-9 residues. *Nat. Immunol.* 3: 1177–1184.
25. Hammer, G. E., F. Gonzalez, M. Champsaur, D. Cado, and N. Shastri. 2006. The aminopeptidase ERAAP shapes the peptide repertoire displayed by major histocompatibility complex class I molecules. *Nat. Immunol.* 7: 103–112.
26. Hammer, G. E., F. Gonzalez, E. James, H. Nolla, and N. Shastri. 2007. In the absence of aminopeptidase ERAAP, MHC class I molecules present many unstable and highly immunogenic peptides. *Nat. Immunol.* 8: 101–108.
27. Yan, J., V. V. Parekh, Y. Mendez-Fernandez, D. Olivares-Villagómez, S. Dragovic, T. Hill, D. C. Roopenian, S. Joyce, and L. Van Kaer. 2006. In vivo role of ER-associated peptidase activity in tailoring peptides for presentation by MHC class Ia and class Ib molecules. *J. Exp. Med.* 203: 647–659.
28. York, I. A., N. Bhutani, S. Zendzian, A. L. Goldberg, and K. L. Rock. 2006. Tripeptidyl peptidase II is the major peptidase needed to trim long antigenic precursors, but is not required for most MHC class I antigen presentation. *J. Immunol.* 177: 1434–1443.
29. Firat, E., L. Saveanu, P. Aichele, P. Staeheli, J. Huai, S. Gaedicke, A. Nil, G. Besin, B. Kanzler, P. van Endert, and G. Niedermann. 2007. The role of endoplasmic reticulum-associated aminopeptidase 1 in immunity to infection and in cross-presentation. *J. Immunol.* 178: 2241–2248.
30. Blanchard, N., T. Kanaseki, H. Escobar, F. Delebecque, N. A. Nagarajan, E. Reyes-Vargas, D. K. Crockett, D. H. Raulet, J. C. Delgado, and N. Shastri. 2010. Endoplasmic reticulum aminopeptidase associated with antigen processing defines the composition and structure of MHC class I peptide repertoire in normal and virus-infected cells. *J. Immunol.* 184: 3033–3042.
31. Nagarajan, N. A., F. Gonzalez, and N. Shastri. 2012. Nonclassical MHC class Ib-restricted cytotoxic T cells monitor antigen processing in the endoplasmic reticulum. *Nat. Immunol.* 13: 579–586.
32. Van Kaer, L., P. G. Ashton-Rickardt, H. L. Ploegh, and S. Tonegawa. 1992. TAP1 mutant mice are deficient in antigen presentation, surface class I molecules, and CD4-8+ T cells. *Cell* 71: 1205–1214.
33. Pérarnau, B., M. F. Saron, B. Reina San Martin, N. Bervas, H. Ong, M. J. Soloski, A. G. Smith, J. M. Ure, J. E. Gairin, and F. A. Lemonnier. 1999. Single H2Kb, H2Db and double H2KbDb knockout mice: peripheral CD8+ T cell repertoire and anti-lymphocytic choriomeningitis virus cytolytic responses. *Eur. J. Immunol.* 29: 1243–1252.
34. Kanaseki, T., N. Blanchard, G. E. Hammer, F. Gonzalez, and N. Shastri. 2006. ERAAP synergizes with MHC class I molecules to make the final cut in the antigenic peptide precursors in the endoplasmic reticulum. *Immunity* 25: 795–806.
35. Delgado, J. C., H. Escobar, D. K. Crockett, E. Reyes-Vargas, and P. E. Jensen. 2009. Identification of naturally processed ligands in the C57BL/6 mouse using large-scale mass spectrometric peptide sequencing and bioinformatics prediction. *Immunogenetics* 61: 241–246.
36. Escobar, H., E. Reyes-Vargas, P. E. Jensen, J. C. Delgado, and D. K. Crockett. 2011. Utility of characteristic QTOF MS/MS fragmentation for MHC class I peptides. *J. Proteome Res.* 10: 2494–2507.
37. Garbi, N., N. Tiwari, F. Momburg, and G. J. Hämmerling. 2003. A major role for tapasin as a stabilizer of the TAP peptide transporter and consequences for MHC class I expression. *Eur. J. Immunol.* 33: 264–273.
38. Aladin, F., G. Lautscham, E. Humphries, J. Coulson, and N. Blake. 2007. Targeting tumour cells with defects in the MHC Class I antigen processing pathway with CD8+ T cells specific for hydrophobic TAP- and Tapasin-independent peptides: the requirement for directed access into the ER. *Cancer Immunol. Immunother.* 56: 1143–1152.
39. van Hall, T., E. Z. Wolpert, P. van Veelen, S. Laban, M. van der Veer, M. Roseboom, S. Bres, P. Grufman, A. de Ru, H. Meiring, et al. 2006. Selective cytotoxic T-lymphocyte targeting of tumor immune escape variants. *Nat. Med.* 12: 417–424.
40. Cifaldi, L., E. Lo Monaco, M. Forloni, E. Giorda, S. Lorenzi, S. Petrini, E. Tremante, D. Pende, F. Locatelli, P. Giacomini, and D. Fruci. 2011. Natural killer cells efficiently reject lymphoma silenced for the endoplasmic reticulum aminopeptidase associated with antigen processing. *Cancer Res.* 71: 1597–1606.
41. Rammensee, H. G., J. Bachmann, and S. Stevanovic. 1997. *MHC ligands and peptide motifs.* Landes Bioscience, Austin, TX.
42. Bouvier, M., and D. C. Wiley. 1994. Importance of peptide amino and carboxyl termini to the stability of MHC class I molecules. *Science* 265: 398–402.
43. Peaper, D. R., and P. Cresswell. 2008. Regulation of MHC class I assembly and peptide binding. *Annu. Rev. Cell Dev. Biol.* 24: 343–368.
44. Praveen, P. V., R. Yaneva, H. Kalbacher, and S. Springer. 2010. Tapasin edits peptides on MHC class I molecules by accelerating peptide exchange. *Eur. J. Immunol.* 40: 214–224.
45. Kloetzel, P.-M. 2001. Antigen processing by the proteasome. *Nat. Rev. Mol. Cell Biol.* 2: 179–187.
46. Lewis, J. W., and T. Elliott. 1998. Evidence for successive peptide binding and quality control stages during MHC class I assembly. *Curr. Biol.* 8: 717–720.
47. Rizvi, S. M., N. Del Cid, L. Lybarger, and M. Raghavan. 2011. Distinct functions for the glycans of tapasin and heavy chains in the assembly of MHC class I molecules. *J. Immunol.* 186: 2309–2320.
48. Chen, M., and M. Bouvier. 2007. Analysis of interactions in a tapasin/class I complex provides a mechanism for peptide selection. *EMBO J.* 26: 1681–1690.
49. Park, B., Y. Kim, J. Shin, S. Lee, K. Cho, K. Früh, S. Lee, and K. Ahn. 2004. Human cytomegalovirus inhibits tapasin-dependent peptide loading and optimization of the MHC class I peptide cargo for immune evasion. *Immunity* 20: 71–85.
50. Kim, S., S. Lee, J. Shin, Y. Kim, I. Evnouchidou, D. Kim, Y. K. Kim, Y. E. Kim, J. H. Ahn, S. R. Riddell, et al. 2011. Human cytomegalovirus microRNA miR-US4-1 inhibits CD8(+) T cell responses by targeting the aminopeptidase ERAP1. *Nat. Immunol.* 12: 984–991.
51. Lybarger, L., X. Wang, M. R. Harris, H. W. Virgin, IV, and T. H. Hansen. 2003. Virus subversion of the MHC class I peptide-loading complex. *Immunity* 18: 121–130.
52. Jiang, Q., H. Y. Pan, D. X. Ye, P. Zhang, L. P. Zhong, and Z. Y. Zhang. 2010. Downregulation of tapasin expression in primary human oral squamous cell carcinoma: association with clinical outcome. *Tumour Biol.* 31: 451–459.

OPEN ACCESS Freely available online

PLOS | ONE

Ectopically Expressed Variant Form of Sperm Mitochondria-Associated Cysteine-Rich Protein Augments Tumorigenicity of the Stem Cell Population of Lung Adenocarcinoma Cells

Akari Takahashi[1,4], Yoshihiko Hirohashi[1]*, Toshihiko Torigoe[1]*, Yasuaki Tamura[1], Tomohide Tsukahara[1], Takayuki Kanaseki[1], Vitaly Kochin[1], Hiroshi Saijo[1], Terufumi Kubo[1], Munehide Nakatsugawa[1], Hiroko Asanuma[2], Tadashi Hasegawa[2], Toru Kondo[3], Noriyuki Sato[1]

1 Department of Pathology, Sapporo Medical University School of Medicine, Chuo-ku, Sapporo, Japan, 2 Department of Surgical Pathology, Sapporo Medical University School of Medicine, Chuo-ku, Sapporo, Japan, 3 Department of Stem Cell Biology, Hokkaido University Graduate School of Medicine, Kita-Ku, Sapporo, Japan, 4 Cancer Diagnosis Laboratory, Japan Science and Technology Agency Innovation Plaza Hokkaido, Japan Science and Technology Agency, Kita-Ku, Sapporo, Japan

Abstract

Cancer stem-like cells (CSCs)/cancer-initiating cells (CICs) are defined as a small population of cancer cells that have self-renewal ability, differentiation ability and high tumor-initiating ability. CSCs/CICs are resistant to cancer therapies including chemotherapy and radiotherapy. Therefore, CSCs/CICs are thought to be responsible for cancer recurrence and distant metastasis after treatment. However, the molecular mechanisms of CSCs/CICs are still elusive. In this study, we isolated CSCs/CICs as side population (SP) cells from lung carcinoma, colon carcinoma and breast carcinoma cells and analyzed the molecular mechanisms of CSCs/CICs. cDNA micro-array screening and RT-PCR analysis revealed that sperm mitochondria-associated cysteine-rich protein (SMCP) is ectopically expressed in SP cells. 5′-Rapid amplification of cDNA end (RACE) analysis revealed that the SMCP transcript in SP cells was a variant form (termed vt2) which is composed from only one exon. SMCP vt2 was detected in only cancer cells, whereas the wild-type (vt1) form of SMCP was expressed in the testis. SMCP was shown to have a role in tumor initiation by SMCP overexpression and SMCP knockdown using siRNAs in lung cancer cells. Taken together, the initiation results indicate that an ectopically expressed variant form of SMCP has a role in tumor initiation of CSCs/CICs and that the variant form of SMCP might be a novel CSC/CIC marker and a potential and promising target of CSC/CIC-targeting therapy.

Citation: Takahashi A, Hirohashi Y, Torigoe T, Tamura Y, Tsukahara T, et al. (2013) Ectopically Expressed Variant Form of Sperm Mitochondria-Associated Cysteine-Rich Protein Augments Tumorigenicity of the Stem Cell Population of Lung Adenocarcinoma Cells. PLoS ONE 8(11): e69095. doi:10.1371/journal.pone.0069095

Editor: Jörg D. Hoheisel, Deutsches Krebsforschungszentrum, Germany

Received February 12, 2013; **Accepted** June 5, 2013; **Published** November 11, 2013

Funding: This work was supported by Grants-in-Aid for Scientific Research from the Ministry of Education, Culture, Sports, Science and Technology of Japan (grant Nos. 16209013, 17016061 and 15659097) for Practical Application Research from the Japan Science and Technology Agency, and for Cancer Research (15-17 and 19-14) from the Ministry of Health, Labor and Welfare of Japan, Ono Cancer Research Fund (to NS) and Takeda Science Foundation (to YH). This work was supported in part by the National Cancer Center Research and Development Fund (23-A-44). The funders had no role in study design, data collection and analysis, decision to publish, or preparation of the manuscript.

Competing Interests: The authors have declared that no competing interests exist.

* E-mail: hirohash@sapmed.ac.jp (YH); torigoe@sapmed.ac.jp (T. Torigoe)

Introduction

Recent progress in cancer research has revealed that cancers are composed of morphologically and phenotypically heterogenous malignant transformed cells, and only a small population of cancer cells have tumor-initiating ability when transplanted into immune-deficient mice (cancer stem cell hypothesis) [1,2]. These cells with high tumorigenicity are called cancer stem-like cells (CSCs)/cancer-initiating cells (CICs). In subsequent works, CSCs/CICs were shown to be resistant to chemotherapies and radiotherapies [3,4]. Therefore, CSCs/CICs are thought to be responsible for disease recurrence after treatments and for distant metastasis, which make the prognosis poor. Thus, eradication of CSCs/CICs is essential for curing cancer.

CSCs/CICs have been isolated by several methods [5], including (1) use of cell surface markers such as $CD44^{+}CD24^{-}$ [6], $CD133^{+}$ [7,8] and $CD166^{+}$ [9], (2) side population (SP) analysis [10], (3) ALDEFLUOR assay [11], and (4) spheroid culture [12]. Using these methods CSCs/CICs have been successfully isolated from acute myeloid leukemia [13–15] breast cancer [6], lung cancer [16], colon cancer [7,8,17], brain tumors [10,18–21], prostate cancer [22–24], pancreas cancer [25,26], liver cancer [27] and melanoma [28]. However, these markers are merely surrogate markers, and sometimes the expression of CSC/CIC markers did not indicate highly tumorigenic CSCs/CICs [29,30]. Therefore, further investigations of CSC/CIC markers and molecular mechanisms of CSC/CIC are needed for the establishment of CSC/CIC targeting therapy.

In this study, we investigated molecular aspects of highly tumorigenic SP cells derived from lung, colon and breast cancer cells and found that a splicing variant form of sperm mitochondria-associated cysteine-rich protein (SMCP), which is expressed in

normal testis tissues, is ectopically expressed in SP cells and that SMCP has a role in the tumor-initiating ability of SP cells. These findings indicate that SMCP might be a novel CSC/CIC marker and a potential target for CSC/CIC targeting therapy.

Materials and Methods

Ethics statement

Mice were maintained and experimented on in accordance with the guidelines of and after approval by the Committee of Sapporo Medical University School of Medicine, Animal Experimentation Center under permit number 10-032. Any animal found unhealthy or sick was promptly euthanized. All studies were approved by Institutional Review Boards (IRB) of Kushiro City General Hospital. We obtained written informed consent from all patients according to the guidelines of the Declaration of Helsinki.

Tissue samples

All studies were approved by Institutional Review Boards (IRB) of Kushiro City General Hospital. Three pairs of lung cancers and adjacent non-neoplastic lung tissues were obtained from surgically resected tissues removed at Kushiro City General Hospital. The histological types of the three cancer tissues were: case #1 and 2, adenocarcinoma; case #3 and 4, squamous cell carcinoma; and case #5, large cell carcinoma.

Cell culture

Lung adenocarcinoma cell line LHK2 was established in our laboratory [31]. Lung small cell carcinoma cell line Lc817 was purchased from the Japanese Cancer Research Resources Bank (Osaka, Japan). Human breast adenocarcinoma cell line MCF7, human lung adenocarcinoma cell line A549 and human embryonal kidney cell line HEK293T were purchased from ATCC (Manassas, VA, USA). Colon adenocarcinoma cell line SW480 [32] was a kind gift from Dr. K. Imai (Sapporo, Japan). These cell lines were cultured in Dulbecco's Modified Eagle's Medium (DMEM) (SIGMA-ALDRICH, St. Louis, MO, USA) with 10% heat-inactivated fetal bovine serum (FBS; MP Biomedicals, Irvine, CA, USA) at 37°C in a humidified atmosphere containing 5% CO_2. The retrovirus packaging cell line PLAT-A was kindly provided by Dr. T. Kitamura (Tokyo, Japan) [33]. PLAT-A was maintained in DMEM containing 10% FBS, 1 μg/mL puromycin (SIGMA-ALDRICH), and 10 μg/mL blasticidin (SIGMA-ALDRICH).

Side population (SP) assay

Side population (SP) analysis was performed as described previously with some modifications [34,35]. The cells were stained with Hoechst33342 dye (Lonza, Walkersville, MD, USA) at final concentrations of 5 μg/ML for LHK2 and SW480 cells and 2 μg/ml for MCF7 cells with or without Verapamil (SIGMA-ALDRICH), an inhibitor of ABC transporters, at the concentration of 75 μM. The cells were incubated at 37°C for 90 min with continuous shaking. Stained cells were analyzed by a FACS Aria II (BD Biosciences, San Jose, CA, USA). The Hoechst 33342 dye was excited at 357 nm and its fluorescence was analyzed using dual wavelengths (blue, 402–446 nm; red, 650–670 nm).

RNA extraction and reverse transcription-PCR analysis

Isolation of RNA and RT-PCR analysis were performed as described previously [36]. Human Multiple Tissue cDNA Panels I and II (TAKARA BIO INC., Otsu, JAPAN) and the Human Fetal Multiple Tissue cDNA Panel (TAKARA BIO INC.) were used as templates of normal adult and fetal tissue cDNA. PCR amplification was performed in 20 μl of PCR mixture containing 1 μl of cDNA mixture, 0.5 μl of Taq DNA polymerase (QIAGEN) and 4 pmol of primers. The PCR mixture was initially incubated at 94°C for 2 min, followed by 35 cycles of denaturation at 94°C for 15 sec, annealing at 58°C for 30 sec, and extension at 72°C for 30 sec. Primer pairs used for RT-PCR analysis were 5′-TGGAGAAGGAGAAGCTGGAGCAAAA-3′ and 5′-GGCAGATGGTCGTTTGGCTGAATA-3′ for *POU5F1* with an expected PCR product size of 163 bps, 5′- GCTGAGATGCCTCACACGGAG-3′ and 5′- TCTGTTTCTTGACGGGACCTTGTC-3′ for *NANOG* with an expected PCR product size of 161 bps, 5′- TGTGTGACCAGACAAAACACAG -3′ and 5′-GTTGGGCTCAGACTCCATGT -3′ for *SMCP* with an expected PCR product size of 249 bps, 5′- TCACTAGGCTGCTGAGGAAGA -3′ and 5′- CTGGGCAGCATTTACTGTGT -3′ for *SMCP-variant1* with an expected PCR product size of 152 bps, 5′-TTCAGGaAGCGTGTGACAGT -3′ and 5′- CTGGGCAGCATTTACTGTGT -3′ for *SMCP-variant2* with an expected PCR product size of 624 bps, and 5′-ACCACAGTCCATGCCATCAC-3′ and 5′-TCCACCACCCTGTTGCTGTA-3′ for *glyceraldehyde-3-phosphate dehydrogenase (GAPDH)* with an expected product size of 452 bps. *GAPDH* was used as an internal control. PCR amplification for *SOX2* was performed with PrimeSTAR HS DNA polymerase (TAKARA BIO INC.). The PCR mixture was initially incubated at 98°C for 2 minutes, followed by 35 cycles of denaturation at 98°C for 15 seconds, and annealing and extension at 68°C for 30 seconds. *SOX2* expression was detected using sense primer 5′-CATGATGGAGACGGAGCTGA-3′ and antisense primer 5′-ACCCCGCTCGCCATGCTATT-3′ with an expected PCR product size of 420 bp.

Quantitative real-time PCR analysis

Quantitative real-time PCR was performed using the ABI PRISM 7000 Sequence Detection System (Applied Biosystems, Foster City, CA) according to the manufacturer's protocol. SOX2 primer and probe was designed by the manufacturer (TaqMan Gene expression assays; Applied Biosystems). Thermal cycling was performed using 40 cycles of 95°C for 15 seconds followed by 60°C for 1 min. Each experiment was done in triplicate, and normalized to the *GAPDH* gene as an internal control.

Microarray analyses

We used the commercially available amino-allyl RNA amplification Kit ver,2 (High Yield Type) (SIGMA-ALDRICH). Purified total RNA (3 μg) was reverse-transcribed to generate double-stranded cDNA using an oligo dT T7 promoter primer and reverse transcriptase. Next, cRNA was synthesized using T7 RNA polymerase, which simultaneously incorporated Cy3- or Cy5-labeled cytidine triphosphate. During this process, the samples of SP cells were labeled with Cy5, whereas the non-SP cells were labeled with Cy3 as control cells. Quality of the cRNA was again checked using the Nano Drop. Cy3-labeled cRNA and Cy5-labeled cRNA were combined and then fragmented in a hybridization cocktail (SIGMA-ALDRICH). Then the labeled cRNAs were hybridized to a 60-mer probe oligonucleotide microarray (Panorama Human Micro Array, SIGMA-ALDRICH) and incubated for 20 h ours at 50°C. The fluorescent intensities were determined by a Genepix 4000B Microarray Scanner (Axon, US). We performed the samples of SP cells were labeled with Cy3 whereas the non-SP cells were labeled with Cy5. Microarray raw data and processed data have been deposited in a ArrayExpress database (http://www.ebi.ac.uk/arrayexpress/, Accession Number: E-MEXP-3913).

5′-Rapid amplification of cDNA ends (5′-RACE) and 3′-RACE

5′ Rapid amplification of cDNA ends (5′-RACE) and 3′-RACE were carried out using total RNA isolated from Lc817 cells to identify the transcriptional start site of the SMCP gene in the cancer cell lines, following the protocol of manufacturer (TAKARA BIO INC.). Briefly, 1 μg of total RNA was utilized to generate either 5′ or 3′ RACE Ready cDNA products with specific primers and reagents provided by the kit in the presence of Moloney Murine Leukemia Virus (MMLV) reverse transcriptase. Generation of the 5′-RACE fragment was performed as described in the protocol. In brief, 50 μl PCR reaction mixture consisting of 2.5 μl of 5′-RACE-Ready cDNA, 5 μl of 10×Universal Primer A Mix (UPM), 1 μl of 10 μM Gene Specific Primer 1 (GSP1) and 41.5 μl of Master Mix (TAKARA BIO INC.) was prepared. Positive and negative controls were prepared according to the protocol of the manufacturer. GSP1 primer, 5′- ATGGCCC-CAGGGACTTCTTCTTTGT-3′, was designed on the basis of nucleotide sequences of SMCP CDS. Nested PCR reaction was done by using diluted 1st PCR production, 1 μl nested universal primer A (NUP) and 1 μl nested GSP1 primer, located upstream of the GSP1 primer, 5′-TGGCCTGGACTCATTTTGTG-GGCTA-3′, instead of the UPM primer and GSP1 primer. In order to generate the 3′ region fragment, 3′-RACE was performed by using a 50 μl PCR reaction mixture cosisting of 2.5 μl of 5′-RACE-Ready cDNA, 5 μl of 10×UPM, 1 μl of 10 uM GSP2, 5′-CTGTGGTTTGGAGACCAAGCCTGAA-3′, and 41.5 μl of master mix. In nested PCR, 1 μl nested GSP2, 5′- ATG-GAGTCTGAGCCCAACTCACCGCAAA-3′, was used. All PCR products were purified and sequences were confirmed by DNA sequencing.

Plasmid construct

The cDNA of human SMCP CDS was isolated from a human testis cDNA library (TAKARA BIO INC.) by PCR, meanwhile splicing variant2 was isolated from lung small cell carcinoma cell line Lc817 by PCR. The SMCP CDS and splicing variant2 was constructed into a pcDNA3.1(+) vector (Life Technologies, Carlsbad, CA, USA), respectively.

Western blotting

Western blotting was performed as described previously [37]. Briefly, HEK293T cells were transfected with SMCP CDS plasmid and splicing variant2 plasmid and then lysed in 1 mL of SDS sample buffer. Anti-SMCP rabbit polyclonal antibody (custum ordered, Life Technologies) was used at 200-times dilution. Anti-β-Actin mouse monoclonal antibody (Sigma, St. Louis, MO, USA) was used at 2000-times dilution.

Mice and xenograft transplantation

Non-obese diabetic-severe combined immunodeficient (NOD/SCID) mice were purchased from Sankyo Laboratory Co. Ltd. (Tsukuba, Japan). Studies were performed with approval of the Animal Experiment Ethics Committee of Sapporo Medical University (Sapporo, Japan).

Various numbers of SP and non-SP cells or LHK2-SMCP and LHK2-Mock cells were suspended in a PBS and Matrigel (BD Biosciences) mixture and transplanted to NOD/SCID mice (female, 4–6 wk of age) under anesthesia. SP and non-SP cells or LHK2-SMCP and LHK2-Mock cells were implanted into the s.c. space on the left and right sides of the back of recipient mice, respectively. Tumor formation was observed weekly for 10–13 weeks. The transplantation assays were performed in accordance with institutional guidelines for the use of laboratory animals.

Generation of GFP-SMCP cell line

The cDNA of human SMCP was isolated from a human testis cDNA library (TAKARA BIO INC.) by PCR. The full-length SMCP was constructed into a pcDNA3.1 (+) vector (Life Technologies, Grand Island, NY, USA) fused with green fluorescent protein (GFP) gene. LHK2 cells were transfected with SMCP-GFP fusion expression plasmid by Lipofectamine 2000 (Life Technologies) and cultured in DMEM supplemented with 10% of FBS and 800 μg/mL Geneticin (Life Technologies).

Generation of stable cell line overexpressing SMCP

Introduction of DNA into LHK2 cells was performed by a retrovirus-mediated method [33]. Briefly, the culture supernatant of PLAT-A cells transduced with the pMXs-based retrovirus vectors containing FLAG-epitope-tagged SMCP, was added onto LHK2 cells in the presence of 8 μg/mL of polybrene (SIGMA-ALDRICH) for 48 hrs. Two days later, the medium was replaced with a fresh medium containing 1 μg/ml puromycin for LHK2 cells to select the infected cells. The mRNA expression of SMCP in the puromycin-resistant sub-line was confirmed by RT-PCR.

Small interfering RNA transfection

SMCP small interfering RNA (siRNA) duplexes were designed and synthesized using the BLOCK-it RNAi designer system (Life Technologies). The oligonucleotide encoding SMCP siRNA1 was 5′- CCCTTAACATGGAGTCTGAGCCCAA -3′, and that encoding siRNA2 was 5′- GCAATCAATGCTGCCCACCA-CAGCA -3′. Cells were seeded at 50% confluence, and transfections were carried out using Lipofectamine RNAiMAX (Life Technologies) in Opti-MEM according to the manufacturer's instructions.

Confocal imaging

LHK2-GFP-SMCP cells were seeded on glass coverslips for 24 hr. The cells were then fixed with 4% paraformaldehyde, permeabilized with 0.1% Triton X-100, and then blocked with 10% goat serum for 40 min. The cells were first stained with MitoTracker Red 580 Dye (Life Technologies) for detecting mitochondria at RT for 20 min and washed. Following this, they were stained with DAPI (Life Technologies) at RT for 5 min and mounted. Each sample was visualized using an LSM510 META ConfoCor3 (Zeiss, Oberkochen, Germany), and images were captured and analyzed using the Zeiss LSM Image Browser (Zeiss).

Statistical analysis

Data are presented as means ± SD. Differences in variables were assessed using Student's t-test. $P<0.05$ was considered significant.

Results

Isolation of CSCs/CICs as SP cells in human lung, breast and colon carcinoma cell lines

SP cells derived from LHK2, SW480 and MCF7 cells are enriched with CSCs/CICs [35,38,39]. We therefore isolated SP cells from LHK2, SW480 and MCF7 cells as CSC/CIC sources. The cells were stained with Hoechst 33342 dye and analyzed with a FACS Aria II flow cytomerter. The rations in LHK2, SW480 and MCF7 cells of SP cells were 1.3%, 1.5% and 0.5%,

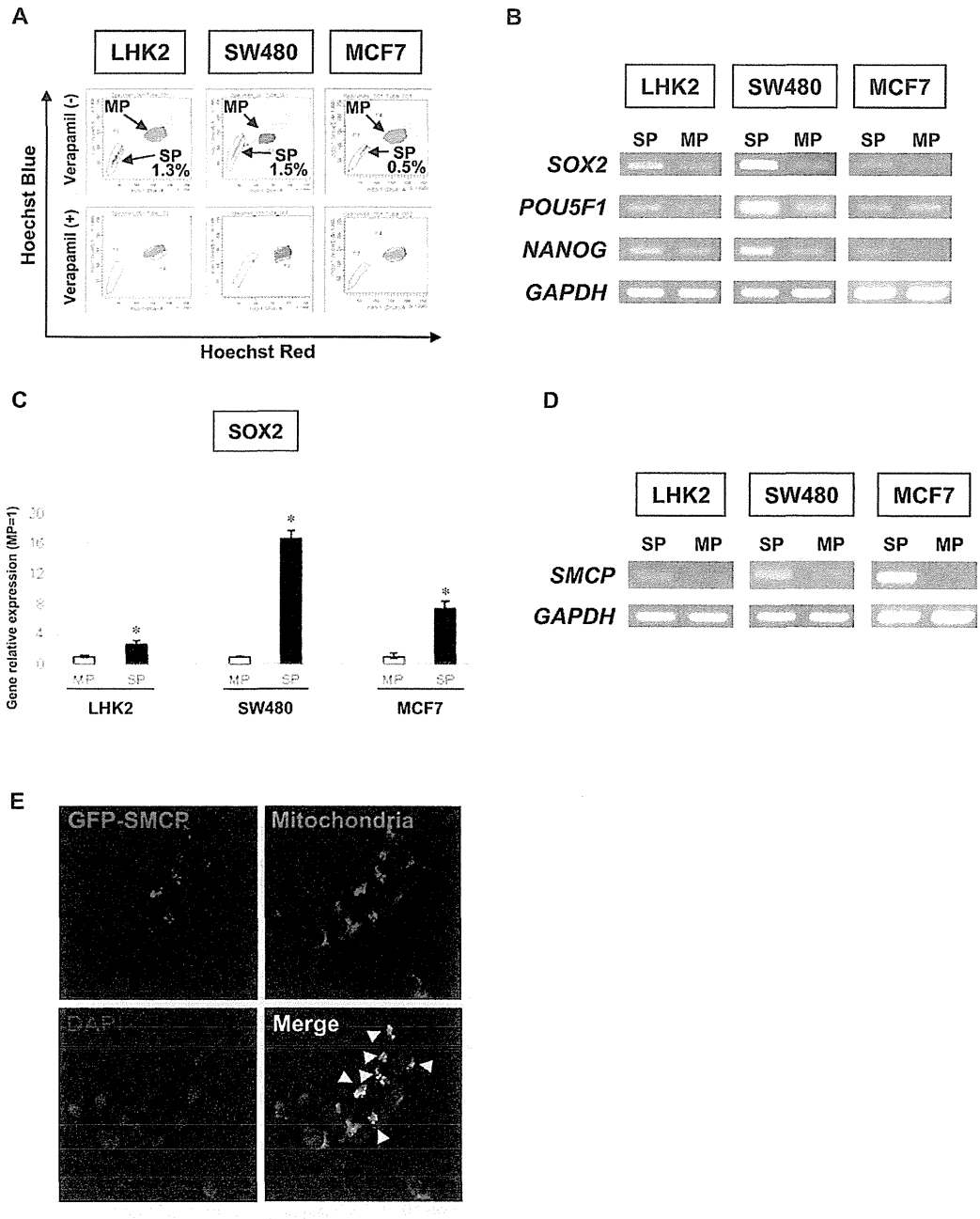

Figure 1. Isolation of a novel CSC/CIC molecule, SMCP. A. Isolation of SP cells from LHK2, MCF7 and SW480 cells. Lung (LHK2), colon (SW480) and breast (MCF7) cancer cells were stained with $Hoechst_{33342}$ dye in the absence (upper panel) or presence (lower panel) of verapamil. All cell lines were analyzed by a cell sorter. **B. Expression profiles of stem cell markers in SP cells and MP cells.** Expression of stem cell markers (*SOX2*, *POU5F1* and *NANOG*) in SP cells and MP cells derived from LHK2, SW480 and MCF7 cells was determined. *GAPDH* was used as an internal positive control. **C. Quantitative real-time PCR analysis of SOX2 mRNA expression in SP and MP cells.** The MP cells were used for the control, which was set as 1.0. Data are expressed as mean + SD of relative values compared to MP cells. **D. Expression of *SMCP* in SP and MP cells.** Expression of *SMCP* in SP cells and MP cells derived from LHK2, SW480 and MCF7 cells was determined. **E. SMCP is localized in mitochondria.** LHK2 cells transfered with GFP-fused SMCP gene were fixed and stained with Mitotracker Red followed by DAPI and then visualized by laser confocal microscopy (Magnification, ×200). Green indicates GFP-fused SMCP. Red indicates mitochondria. Blue indicates nucleus.
doi:10.1371/journal.pone.0069095.g001

Table 1. Tumor-initiating ability of SP and MP cells.

MCF7		Cell numbers of injection into NOD/SCID mice			
Day 91 post injection		**1.5×10^1**	**1.5×10^2**	**1.5×10^3**	**1.5×10^4**
SP cells	Incidence	1/1	1/1	1/1	n.d.
	Volumes (mm^3)	0.5	683.6	288.8	-
MP cells	Incidence	0/1	0/1	1/1	1/1
	Volumes (mm^3)	-	-	165.5	691.9
SW480		**Cell numbers of injection into NOD/SCID mice**			
Day 42 post injection		**1.0×10^1**	**1.0×10^2**	**1.0×10^3**	**1.0×10^4**
SP cells	Incidence	1/3	1/3	3/3	3/3
	Volumes (mm^3)	40	720	1225±571.7	7167±2020
MP cells	Incidence	0/3	1/3	3/3	3/3
	Volumes (mm^3)	-	50	281±129	2789±1910

Incidence indicates the number of tumor formation/number of injections.
Tumor volumes are mean±S.D.
doi:10.1371/journal.pone.0069095.t001

respectively (Figure 1A). Greater tumor-initiating ability of SP cells was confirmed by injecting NOD/SCID mice with the cells (Table 1) [38]. To address the expression levels of stem cell markers in SP cells, we performed RT-PCR analysis. *SOX2*, *POU5F1* and *NANOG* were expressed in SP cells derived from LHK2, SW480 and MCF7 cells at higher levels than those in MP cells (Figure 1B). Moreover, we evaluated three mRNA transcripts with quantitative real-time PCR. As shown in figure 1C, *SOX2* mRNA was significantly overexpressed in SP cells compared with MP cells. The results indicated that these SP cells had molecular properties similar to those of iPS cells [40].

Sperm mitochondria-associated cysteine-rich protein (SMCP) is preferentially expressed in SP cells

To address the molecular mechanism of SP cells, we performed gene chip microarray screening using total RNA from LHK2 SP cells and LHK2 MP cells (Table S1). We found that *SMCP* gene oligo reactive mRNA was overexpressed in LHK2 SP cells compared with the expression level in LHK2 MP cells. RT-PCR analysis revealed that *SMCP* mRNA was overexpressed in SP cells derived from LHK2, SW480 and MCF7 cells compared to the expression levels in MP cells (Figure 1D). Since the SMCP protein was reported to be expressed in sperm mitochondria [41], the cellular localization of SMCP in cancer cells was investigated using a GFP-fused SMCP gene. Co-localization of GFP-fused SMCP and a mitochondria marker (MitoTracker) was observed in LHK2 cells with overexpressed GFP-SMCP gene, indicating that ectopically expressed SMCP protein is also localized in mitochondria (Figure 1E).

Expression profiles of SMCP in normal tissues and cancer cells

RT-PCR analysis was performed to determine the expression of *SMCP* in human fetal and adult normal tissues and in cancer cells. *SMCP* mRNA was expressed only in the testis at a high level among human adult tissues (Figure 2A). *SMCP* mRNA was detected in all cancer cells tested in this study, including renal cell carcinoma cells (Caki-1, ACHN, SMKT-R1, SMKTR-2, SMKTR-3 and SMKTR-4), lung squamous cell carcinoma cells (Sq-1), lung small cell carcinoma cells (Lc817), lung large cell carcinoma cells (86-2 and Lu99), lung adenocarcinoma cells (1-87 and A549) and pancreas carcinoma cells (HPC3) (Figure 2B). *SMCP* mRNA was preferentially expressed in primary lung cancerous tissues in 5 cases (2 adenocarcinomas, 2 squamous cell carcinomas and 1 large cell carcinoma) than those in adjacent normal counterpart lung tissues (Figure 2C).

Novel SMCP splicing variant2 is the dominant form in cancer cells

The SMCP transcript is composed of two exons (Variant 1, Figure 2D upper panel), and we tried to detect the SMCP transcript by quantitative PCR (qPCR) using a probe designed at the junction of exon 1 and exon 2. We detected *SMCP* mRNA in the testis tissue, but we did not detect *SMCP* mRNA in any of the cancer cells by qPCR. We therefore hypothesized that the transcript of SMCP in cancer cells was different from that in the testis. To address the structure of *SMCP* mRNA, we performed 5′ RACE and 3′ RACE. The cDNA template used was prepared from the Lc817 cell line, which showed a high level of *SMCP* transcript (Figure 2B). The 5′ RACE PCR amplification revealed that the *SMCP* mRNA from Lc817 is composed of only one exon that is overlapped with exon 2 with 5′ extension (termed SMCP variant 2) and shares coding sequence (CDS) (Figure 2D). We therefore analyzed the SMCP mRNAs in testis and cancer cells using a mixture of SMCP variant1-specific primer (F1) and SMCP variant2-specific primer (F2), and we found that SMCP vt1 is expressed in the testis and that SMCP vt2 is expressed in cancer cells (Figure 2E). We could detect a specific band with anti-SMCP polyclonal antibody in the HEK293T cell line transfected with expression vectors of both variant2 and variant1 CDS (Fig. 2F), suggesting that both variant1 and variant2 have the same protein products. We therefore used CDS expression constract for further analyze of SMCP functions.

SMCP has a role in tumor-initiating ability

Since SMCP is preferentially expressed in SP cells, we further analyzed the function of SMCP using SMCP-overexpressing cells. SMCP cDNA was stably transduced into LHK2 cells, and its expression was confirmed by RT-PCR (Figure 3A). A tumor was initiated by 1×10^2 LHK2-SMCP cells in 1 of 5 mice, and tumors were initiated by 1×10^3 and 1×10^4 LHK2-SMCP cells in 3 of 5

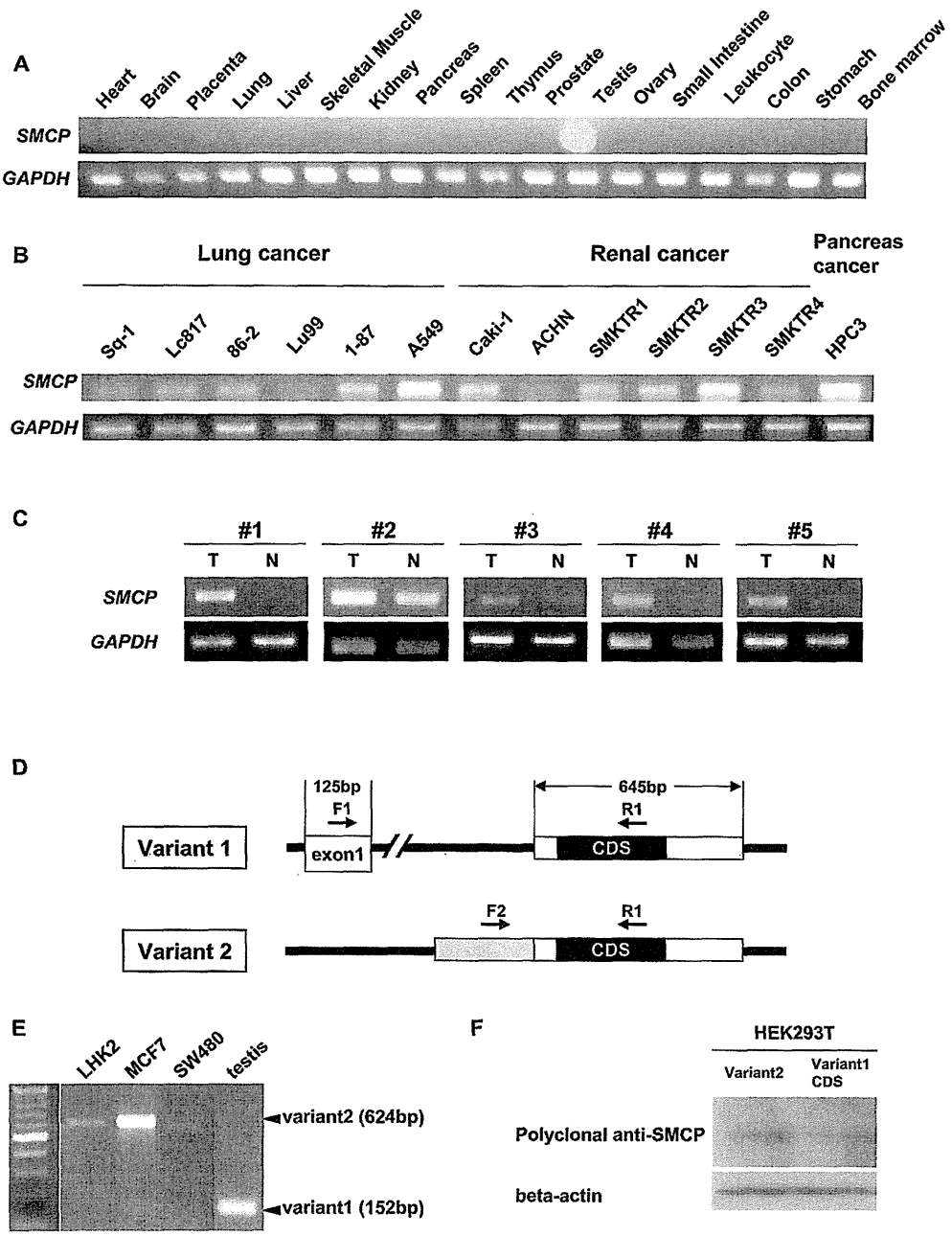

Figure 2. Expression profiles of SMCP and identification of a novel variant form of SMCP. A. SMCP expression profiles in normal human organs. SMCP mRNA expression in normal tissues (heart, brain, placenta, lung, liver, skeletal muscle, kidney, pancreas, spleen, thymus, prostate, testis, ovary, small intestine, leukocyte, colon, stomach and bone marrow) was investigated by RT-PCR. cDNAs were obtained from TAKARA BIO INC. (Human Multiple Tissue cDNA Panels I and II). *GAPDH* was used as an internal positive control. **B. SMCP expression profiles in human cancer cells.** SMCP mRNA expression in lung cancer line cells (Sq-1, Lc817, 86-2, Lu99, 1-87, A549), renal cancer line cells (Caki-1, ACHN, SMKTR1, SMKTR2, SMKTR3, SMKTR4) and pancreas cancer line cell (HPC3) was investigated by RT-PCR. cDNAs were generated by total RNAs derived from cell lines. *GAPDH* was used as an internal positive control. **C. SMCP expression profiles in human lung cancer tissues.** *SMCP* mRNA expression in human lung cancer tissues was investigated by RT-PCR. #1 and #2 are adenocarcinoma cases. #3 and #4 are squamous cell carcinoma cases. #5 is a large cell carcinoma case. T indicates lung cancer tissue. N indicates adjacent lung normal tissue. *GAPDH* was used as an internal positive control. **D. Schema of novel variant form of SMCP.** SMCP wild type (variant 1) is composed of exon 1 and exon 2. The novel isoform of SMCP (variant 2) has only one exon with a 5′ terminal additional extension. **E. Expression profiles of SMCP variant 1 and variant 2 in the testis and cancer cells.** SMCP mRNA expression was investigated by RT-PCR using an F1 and F2 mixture primer as a forward primer and R1 primer as a reverse primer in testis and cancer cells. Variant 1 was a 152-bp PCR product, and variant 2 was a 624-bp PCR product. **F. Expression of SMCP protein.** Detection of SMCP protein in HEK293T cells transfected with expression vectors of variant1 CDS and variant2 as assessed by Western blot analysis with polyclonal SMCP antibody. Beta-actin was used as a protein loading control.
doi:10.1371/journal.pone.0069095.g002

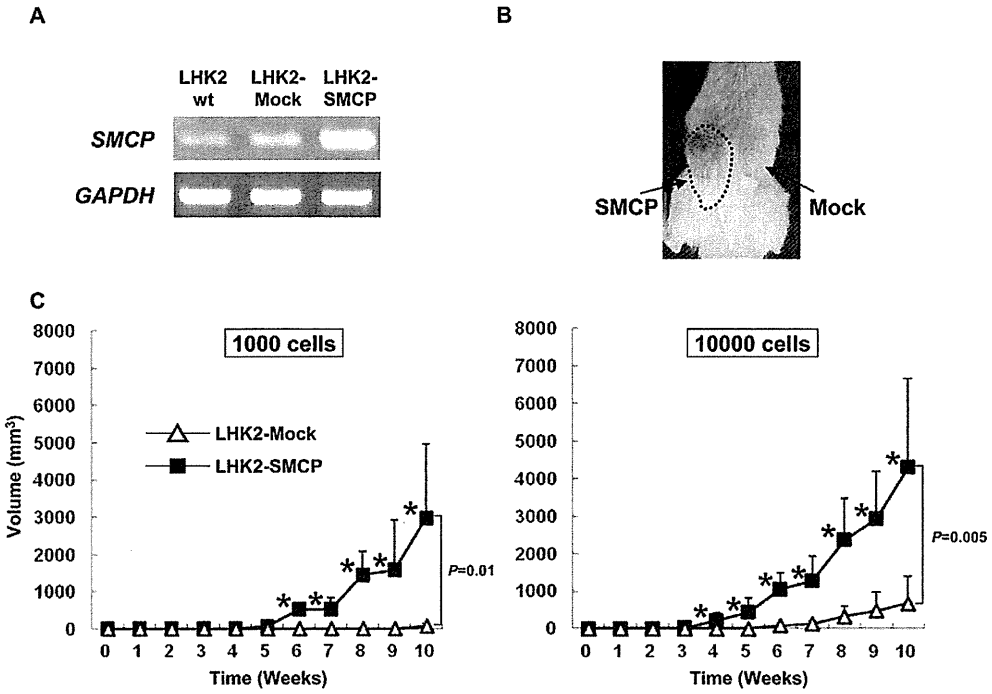

Figure 3. SMCP has a role in the tumor-initiating ability in LHK2 lung adenocarcinoma cells. A. Expression of SMCP in SMCP-overexpressed LHK2 cells. Expression of SMCP in LHK2-SMCP cells was confirmed by RT-PCR. **B. Representative picture of tumors injected with SMCP-overexpressed LHK2 cells. C. Tumor growth of LHK2-SMCP cells and LHK2-Mock cells.** One×10^3 and 1×10^4 of LHK2-SMCP cells and LHK2-Mock cells were injected into NOD/SCID mice subcutaneously. Data are means + SD. Asterisks represents statistical significant difference. Student's t-test. $P<0.05$.
doi:10.1371/journal.pone.0069095.g003

mice and 5 of 5 mice, respectively. On the other hand, a tumor was initiated by 1×10^4 LHK2-Mock cells in 3 of 5 mice, and no tumor initiation was observed with 1×10^2 or 1×10^3 LHK2-Mock injection (Table 2). Furthermore, the growth of tumors derived from LHK2-SMCP cells was significantly faster than that of tumors derived from LHK2-Mock cells (Figure 3B and 3C).

Downregulation of SMCP by siRNA abrogates tumor-initiating ability of wild-type and SP cells of lung cancer cells

The results obtained by using SMCP-overexpressing cells suggested that SMCP has a role in tumor initiation, and we therefore performed a gene knockdown study using siRNAs. We designed two different siRNAs and confirmed gene knockdown by RT-PCR using SMCP siRNA-transfected LHK2 cells (Figure 4A). To investigate the tumor-initiating ability of SMCP knockdown cells, we injected SMCP siRNA-transfected LHK2, Lc817 and A549 cells into NOD/SCID mice. Tumor growth was significantly suppressed in mice injected with SMCP siRNA1 and siRNA2-transfected LHK2, Lc817 and A549cells compared to that in mice injected with control siRNA-transfected LHK2 cells (Figure 4B and 4C and table 3).

Since *SMCP* was preferentially expressed in SP cells, we therefore performed gene knockdown using SP cells derived from wild type LHK2 cells. Two hundred siRNA-transfected LHK2 SP

Table 2. Tumor-initiating ability of LHK2-SMCP and LHK2-mock.

		Cell numbers of injection into NOD/SCID mice			
Day 35 post injection		**1×10^1**	**1×10^2**	**1×10^3**	**1×10^4**
LHK2-SMCP	Incidence	0/5	1/5	3/5	5/5
	Volumes (mm^3)	-	4.0	57.3±43.9	436.3±386.2*
LHK2-mock	Incidence	0/5	0/5	0/5	3/5
	Volumes (mm^3)	-	-	-	4.83±7.5

Incidence indicates the number of tumor formation/number of injections.
Tumor volumes are mean±S.D.
*P<0.01, compared with tumor volumes of 1×10^4 Mock cells.
LHK2-SMCP, SMCP-overexpressing LHK2 cells; LHK2-mock, mock-transfected cells.
doi:10.1371/journal.pone.0069095.t002

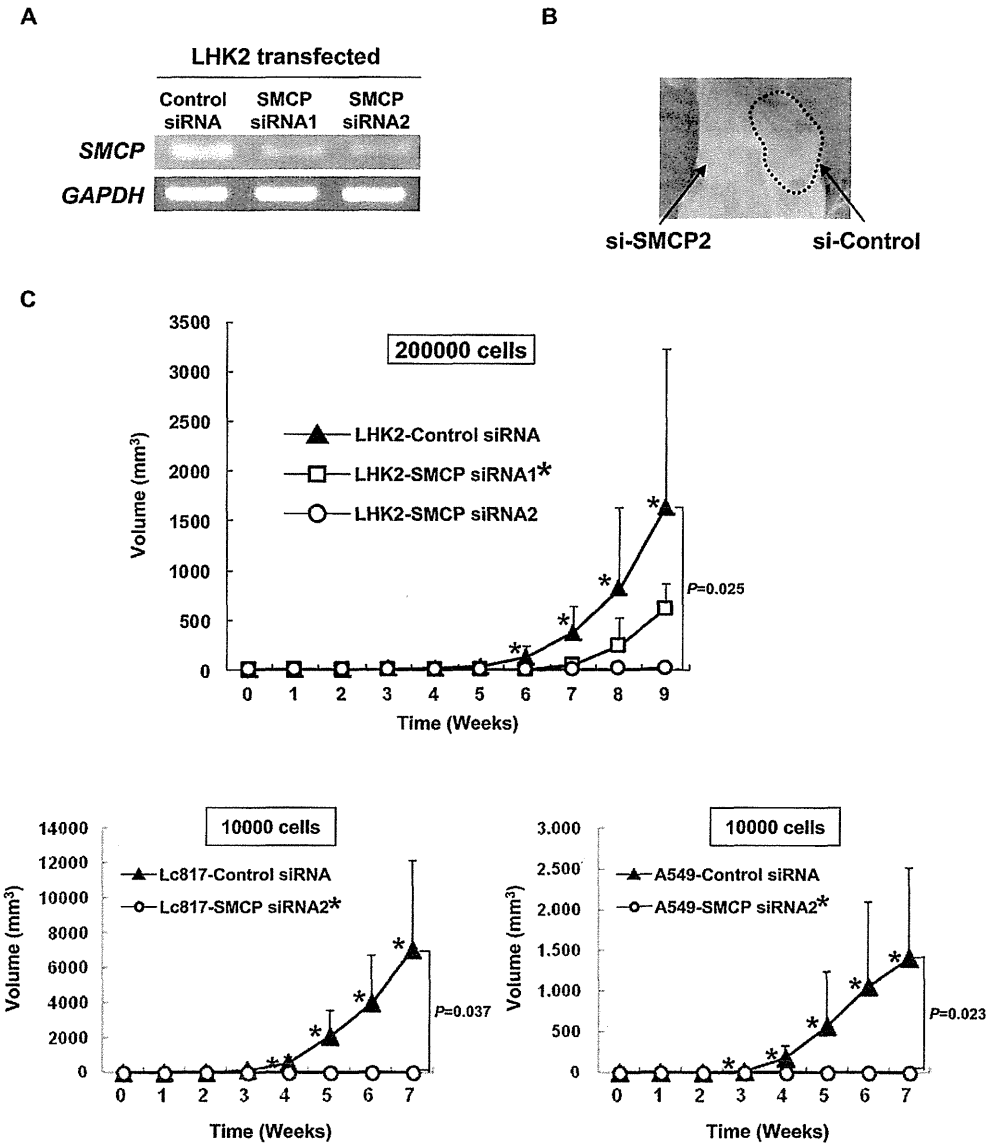

Figure 4. SMCP knockdown abrogates tumor initiation of LHK2 cells. A. Downregulation of SMCP expression in LHK2 cells transfected with siRNA. B. Representative picture of tumors injected with SMCP knockdown LHK2 cells. C. Tumor growth of LHK2, A549 and Lc817 cells transfected with SMCP siRNAs. Two×10^5 LHK2 cells transfected with control siRNA or SMCP siRNA 1 and 2 were injected into NOD/SCID mice subcutaneously. One×10^4 A549 cells transfected with control siRNA or SMCP siRNA2 were injected into NOD/SCID mice subcutaneously. One×10^4 Lc817 cells transfected with control siRNA or SMCP siRNA2 were injected into NOD/SCID mice subcutaneously. Data are means + SD. Asterisks represents statistical significant difference. Student's t-test. $P<0.05$.
doi:10.1371/journal.pone.0069095.g004

cells were injected into the backs of NOD/SCID mice. Control siRNA-transfected LHK2 SP cells initiated tumors, whereas SMCP siRNA-transfected LHK2 SP cells did not initiate tumors (Figure 5). Taken together, these results indicate that SMCP has a role in the tumor-initiating ability of CSCs/CICs.

Discussion

In this study, we investigated the gene expression profile of SP cells derived from LHK2 lung adenocarcinoma cells. The existence of CSCs/CICs has been discussed widely over the past decade [40,41][42]. The concept of stem cell-like tumor cells is intriguing; however, identification and isolation of such cells is difficult. Stem cells are identified by expression of surface markers or functional markers such as ABC transporters or ALDH, and clonogenic potential and capacity to regenerate tumors of the identified subset of tumor cells are subsequently demonstrated [42]. Although the field of CSC/CIC biology is a relatively new field, continued elucidation of the features of these cells holds promise for the development of novel patient therapies [42][43]. Moreover, evidence supporting the existence of CSCs/CICs in various solid tumors has been obtained; however, a definite CSC/

Table 3. Tumor-initiating ability of SMCP siRNA and Control siRNA.

LHK2		Cell numbers of injection into NOD/SCID mice		
Day 35 post injection		**Contorl siRNA**	**SMCP siRNA1**	**SMCP siRNA2**
2×10^5	Incidence	6/6	2/5	0/5
	Volumes (mm^3)	27.8±15.7	0.9±1.7*	-
Lc817		**Cell numbers of injection into NOD/SCID mice**		
Day 28 post injection		**Contorl siRNA**	**SMCP siRNA1**	**SMCP siRNA2**
1×10^4	Incidence	3/4	-	0/4
	Volumes (mm^3)	541.1±299.2	-	0.0±0.0†
A549		**Cell numbers of injection into NOD/SCID mice**		
Day 28 post injection		**Contorl siRNA**	**SMCP siRNA1**	**SMCP siRNA2**
1×10^4	Incidence	4/4	-	0/4
	Volumes (mm^3)	176.6±147.4	-	0.0±0.0†

Incidence indicates the number of tumor formation/number of injections.
Tumor volumes are mean±S.D.
*$P<0.01$, compared with tumor volumes of 2×10^5 Control siRNA cells.
†$P<0.05$, compared with tumor volumes of 1×10^4 Control siRNA cells.
doi:10.1371/journal.pone.0069095.t003

CIC marker has not yet been established. Attempts to enrich CSCs/CICs by using SP analysis have been made in several studies [10,35,38,44–47]. In this study, we succeeded in isolating SP cells from LHK2 lung carcinoma cells, SW480 colon carcinoma cells and MCF7 breast carcinoma cells. SP cells exhibited greater tumor-initiating ability and higher expression levels of iPS cell-related genes (SOX2, POU5F1 and NANOG), indicating that SP cells derived from LHK2, SW480 and MCF7 cells are enriched with CSCs/CICs and are a reasonable source for further research.

Gene expression profiling using cDNA microarrays and RT-PCR analysis revealed that the sperm-related gene *SMCP* is ectopically expressed in SP cells derived from LHK2, SW480 and MCF7 cells. Several molecular mechanisms of cancer stem cells have been described. Weinberg's group described that breast cancer stem cells also have epithelial-mesenchimal transition (EMT) phenotypes [48]. However, we did not detect any EMT related genes by cDNA microarray. SOX2 have been showed to be related to lung carcinogenesis, and we also found that SOX2 was overexpressed in LHK2 SP cells [49] [50] [38]. Other report

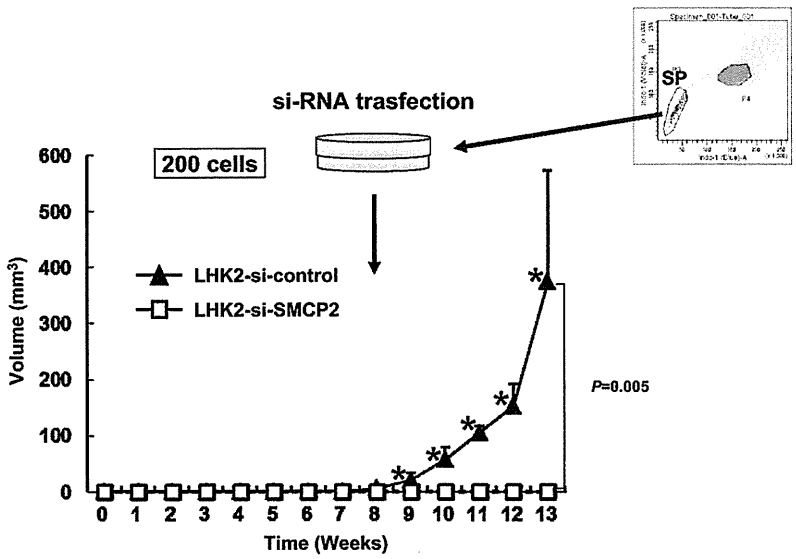

Figure 5. SMCP knockdown abrogates tumor initiation of LHK2 SP cells. LHK2 SP cells were isolated and seeded onto a 24-well plate. SMCP siRNA was transfected into LHK2 SP cells. Two days after transfection, LHK2 SP cells were injected into NOD/SCID mice. Data are means + SD. Asterisks represents statistical significant difference. Student's t-test. $P<0.05$.
doi:10.1371/journal.pone.0069095.g005